Department of Precision and Microsystems Engineering

An innovative concept for airpot based passive vibration isolation

N.J. Velders

Report no : 2017.061
Coach : J.W. Spronck
Professor : J.L. Herder
Specialisation : Mechatronic System Design
Type of report : Master Thesis
Date : 15-12-2017

Contents

List of Tables

List of Figures

Nomenclature

δ	Disturbance
Δ_p	Change in volume due to distrurbance
ω_n	Natural frequency
ζ	Damping factor
A	Area
A_a	Area of the add-on piston
A_g	Area of the ground-airpot interface
A_p	Area of the main piston
ca_x	Extra damping value for the add-on
ca_z	Extra damping value for the main piston
D_a	Diameter of the add-on piston
D_g	Diameter of the ground-airpot interface
D_p	Diameter of the main piston
f_n	Natural frequency
Fz_{spring}	Spring stiffness in z-direction
g	Gravitational constant
k_s	Spring stiffness
k_z	Stiffness in z-direction
ka_x	Extra damping value for the add-on
ka_z	Extra damping value for the add-on
kp_x	Stiffness of the add-on piston due to airpot characteristic
kp_z	Stiffness of the add-on piston due to airpot characteristic
L_0	Initial length of a spring
L_p	Pre-tensioning distance of a spring
M	Mass ontop of the main piston

m	Mass of the add-on piston
p_0	Initial pressure of the airpot
p_a	Armospheric pressure
p_{in}	Absolute pressure inside the airpot
r	Adiabatic Index
V	Volume of the airpot
V_0	Initial volume of the airpot

Chapter 1

Summary

This graduation project was aimed to improve on a vibration isolation technique that is currently often used in the high precision industry. This vibration isolation technique is called the airspring or airpot. It consists of a pressurised vessel that can carry a large mass (such as a measurement table, capable of carrying a load of several 100 kilograms) and has isolation characteristics that reduce the impact of ground vibrations on the setup. The general idea of this improvement is to add an additional piston by modifying an existing setup (can be any airpot) and thereby changing the characteristics of that airpot to improve the vibration isolation capabilities.

In this report the first steps towards such an additional piston, or add-on, are presented and discussed. These first steps consist of an analytical model and a test setup. The analytical model is build using a method called Signal Glow Graph Theory, because conventional model building (free body diagrams with Laplace transformation) was not found to be able of capturing the single input multiple-output characteristics imposed by the addition of the proposed add-on. The purpose for the test setup is twofold, to validate the model and to act as a demonstrator.

The working principle is based upon Newton's second law, which says that a lower mass will accelerate faster. The purpose of the add-on is to keep the pressure inside the pot constant, mitigating the force deviations on the main piston. The add-on is thus designed with a small mass such that it will quickly react to perturbations in the pressure thereby reducing the force deviations on the main piston.

As this was the first demonstrator and there was a desire for many tuneability options, this demonstrator is mostly 3D-printed and build up of basic (home depot - available) parts. This caused some problems with leakage, and for a final product the fabrication should be different. This demonstrator was successfully built and measurements were made for validation.

Due to time limitations the demonstrator was not equipped with an add-on, but serves to validate part of the model. The fabrication of the demonstrator gave insights into the fabrication process of airpots, which can be used in further research. It was shown that the model works correctly, keeping in mind the limits of the demonstrator. A validated model is realised to study the potential improved vibration isolation with the add-on concept. According to the model, the add-on concept is indeed able to improve state of the art airpots in the frequency range where normal airpots show a resonance peak 1-10 Hz. When this research will be continued, products could be developed for either in-house use to assist the research done at the Precision and Microsystem (PME) research group, or be developed in a commercial product.

Chapter 2

Introduction

2.1 Background

As the technology keeps advancing, the trend of miniaturization continues. When the scale decreases, influences that could previously be neglected could become very troublesome. Especially when the amplitude is near the desired dimension of operation [1], for example when something needs to be positioned on a micrometer scale, vibrations of a few micrometers might cause very large issues. The technology which acts on this very small scale is often referred to as (High) Precision Mechanisms. [1][2]

To adequately do measurements and testing on high precision mechanisms it is key that external influences are isolated or at least minimized to a level where they do not cause significant errors on the results. One of these external sources are ground vibrations. These vibrations are caused by all kinds of external sources, for example by nearby traffic, equipment in the room or a closing door. Hence there is a need to isolate or reduce these disturbances from the high precision mechanism. Different solutions are already available, section 3.2, but as the technology keeps advancing and the scale keeps declining, the need for improvements in vibration isolations solutions also continues.

One of the more regular used solutions to deal with these vibrations is the air-spring, also known as an airpot. In such a system a closed air pocket acts as a spring on which a piston with the load is resting, a picture is shown in figure 2.1. However these solutions show a resonance peak in the 1-10 Hz frequency range which is undesirable. An idea to improve on this principle is to add an add-on with zero-stiffness behaviour which will passively deal with the external vibrations. This idea is the basis of this research and is further explained in section 4.

2.2 Research goals and objectives

The goal of this study is (1) to model the effect of the suggested solution on an existing product, (2) to theoretically show what improvement can be made on the state of the art systems and (3) to verify that the obtained model is correct. A main focus of this research is on the 1-10 Hz

Figure 2.1: An example of an airpot [1]

frequency range, in which current solutions show a resonance peak that is undesired.

2.3 Structure of the thesis

This thesis is structured as follows: in chapter 3 the theory is listed for the different areas of interest for this thesis work, chapter 5 shows the modelling and the there from derived parameters that results in an optimal design of the system. To validate this model, a demonstrator was designed and tested. This is shown in chapter 6. The model and the measurement results from the demonstrator are compared in chapter 7. The conclusions and recommendations from this thesis work are shown in chapter 8.

[1] https://www.newport.com/mam/celum/celum_assets/S-2000_black-S_800w.jpg?1, March 2017

Chapter 3

State of the Art

In this chapter an introduction into vibration isolation is given (section 3.1). In section 3.2 the products currently available on the market are shown, these products give a reference performance for the results in this thesis.

3.1 Introduction into vibration isolation

According to [3], vibration isolation can be described as: *"Vibration isolation concerns means to bring about a reduction in a vibratory effect. A vibration isolator in its most elementary form may be considered as a resilient member connecting the equipment and foundation. The function of an isolator is to reduce the magnitude of motion transmitted from a vibrating foundation to the equipment or to reduce the magnitude of force transmitted from the equipment to its foundation."*

3.1.1 Vibration sources and characteristics

Sources of vibration can be divided into 3 main categories; Ground-, acoustic- and direct force disturbances. Ground vibrations enter through the foundation of the setup (vibrating floors, closing doors, people walking by). Acoustic vibrations are transmitted through the air and are generally dominant above 50 Hz. [4] The third vibration source, direct force disturbances, are caused either by mechanical coupling to a setup or through internal vibrations of the setup. The focus of this research project is on ground vibrations. Ground vibrations are classified due to different operating environments. They are classified into different levels as shown in figure 3.1.

3.1.2 Performance of vibration isolation solutions

Performance of vibration isolation systems is usually done by means of a Bode plot. A bode plot is a graphical representation of the response of a system for certain frequencies. Horizontal axis is frequency, usually in Hertz or radians per second, on the vertical axis the magnitude of

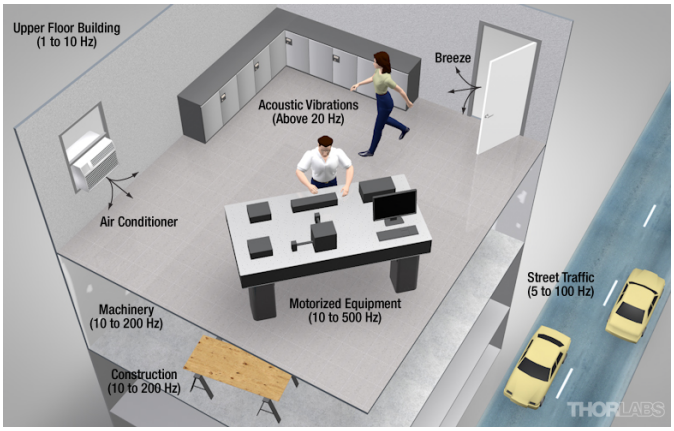

Figure 3.1: Different sources of ground vibrations[1]

the response is displayed on a logarithmic scale, either in actual values but more commonly in decibels. An example is shown in figure 3.2.

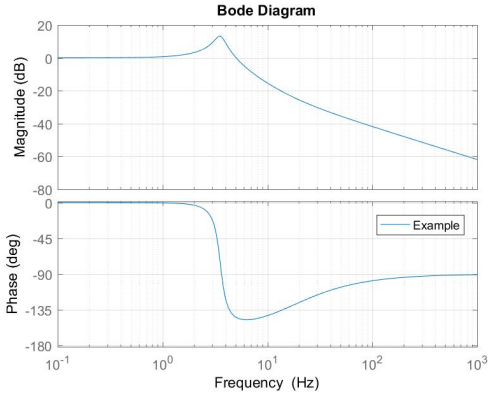

Figure 3.2: Example of a transmissibility curve

3.2 Products available on the market

On the market two categories of high-performance vibration isolation are found; pneumatic solutions and mechanical spring solutions. Another distinction that can be made is that between passive vibration isolation and active vibration isolation. The focus of this research is on the passive vibration isolation solutions. But active solutions are also shown as it would be a great achievement if the proposed add-on concept would out-perform the active solutions.

[1] `https://www.thorlabs.de/newgrouppage9.cfm?objectgroup\_id=8275`, February 2016

3.2.1 Pneumatic solutions

Pneumatic vibration isolation solutions are usually referenced to as "airpots", or "airsprings". This type of solution for vibration isolation which uses a pocket of over-pressurized air for both the required force to lift the table and decrease the transmissibility of ground vibrations. A schematic is shown in figure 3.3a. Current airpots on the market have a peak in the 1-10 Hz range, as can be observed in figure 3.4a. For frequencies around this peak the transmissibility is larger than one. This means that disturbances in that frequency range are amplified instead of reduced, to opposite of the goal of vibration isolation. Damping can be increased to reduce the peak, but this will lower the isolation performance on the higher frequencies.

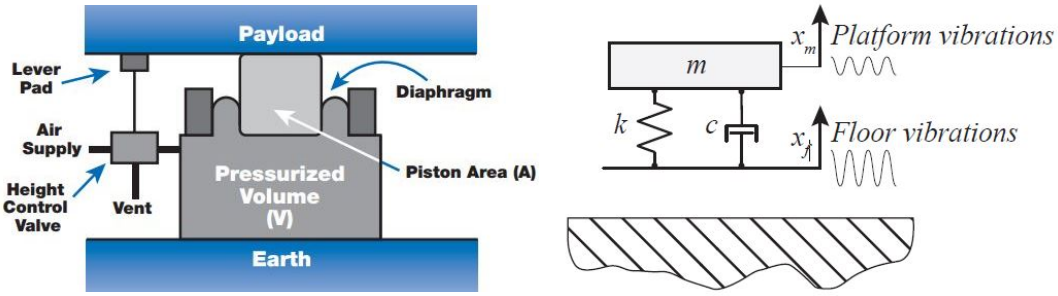

(a) A visualization of the air-spring concept [4]

(b) Mass-Spring-Damper Model

Figure 3.3: Basic air spring

Performance

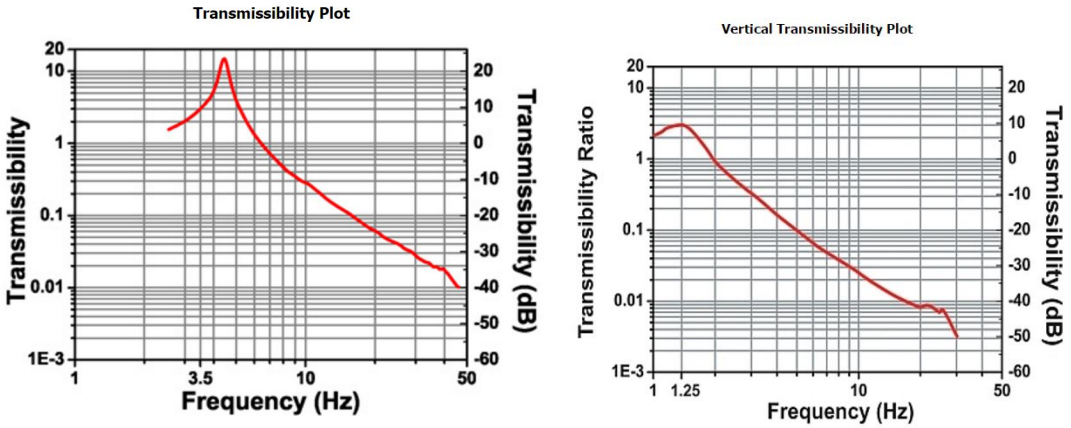

(a) Transmissibility of the Thorlabs passive system[2]; resonance at 4.5 Hz, 22 dB(PTP702, 55% load)

(b) Thorlabs Transmissibility active[3]; resonance at 1.25 Hz, 10 dB

Figure 3.4: Transmissibility of the Thorlabs solutions.

[2] https://www.thorlabs.com/newgrouppage9.cfm?objectgroup_id=1105, Jun 2017
[3] https://www.thorlabs.com/newgrouppage9.cfm?objectgroup_id=1095, Jun 2017

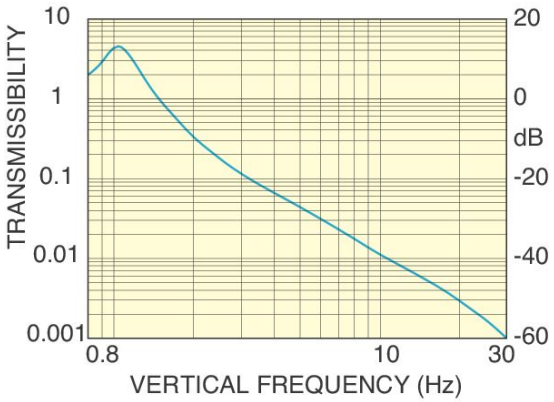

Figure 3.5: Newport Transmissibility active[4]; resonance at 1 Hz, 10 dB, (S-2000A-116)

3.2.2 Mechanical spring solutions

Another type of vibration isolator is based on a smart spring configuration. The load (of a measurement table) is supported with a large spring with a high stiffness. Additional springs are pre-loaded and used to apply a negative stiffness in the vertical direction, the concept is visualized in figure 3.6a. This concept offers lower resonance frequencies than most airspring concepts, but a resonance peak still remains as shown in 3.6b.

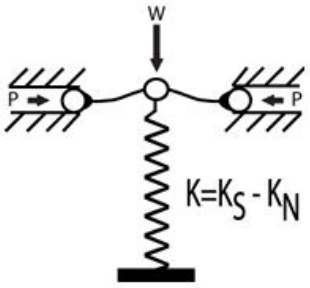

(a) Visualisation of the mechanical spring concept

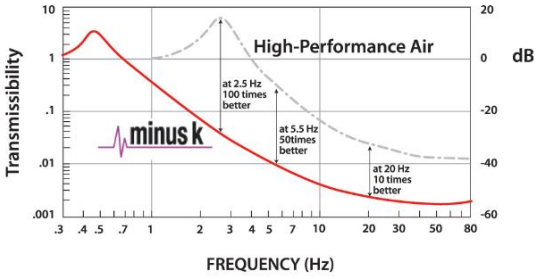

(b) Transmissibility of Minus K system

Figure 3.6: A mechanical spring based vibration isolation solution [15]

[4] https://www.newport.com/mam/celum/celum_assets/I-2000_Vert_Trans-S_600w.gif?1

Chapter 4

Research Framework

4.1 Introduction

In this chapter the concept of the add-on solution is explained in more detail 4.2. To obtain a good understanding of airpots the "known" formulas are derived in section 4.3. Also some additional options and challenges are discussed for such an add-on; the possibility of using magnetism in section 4.4 and the potential issue with atmospheric pressure deviations in section 4.5.

4.2 Working principle of the add-on

In a normal airpot a ground vibration will increase the pressure inside the airpot, which will apply an extra force on the piston with the mass, which in turn will cause the mass on top of the airpot to accelerate. This is shown in figure 4.1. This acceleration is undesired. The general idea of the improved airpot is shown in figure 4.2, where the additional piston will take care of the pressure deviations. An acceleration of this piston will have no direct effect on the equipment on top of the table.

In an ideal situation the add-on will mitigate the pressure deviations instantly. To do this it would theoretically have to have zero-mass and a zero-stiffness (constant force) range which would greatly improve the vibration isolation of the airpot. However this is not realistic. In reality there will be some reaction time and the main piston will also experience a force change. If the add-on would really have a zero-stiffness the add-on would be pushed towards the edges of its working range before equilibrium is again obtained. Therefore a small stiffness is required to keep the add-on piston (and the main-piston) working around their designed working point.

From this some assumptions and requirements for the add-on can be made. 1) the potential volume-change provided by the add-on should be large enough to deal with the pressure deviations. 2) To react quickly to pressure deviations we would like to keep the mass (m_a) as small as possible. 3) We would require some damping as not to have an oscillating add-on piston which could have a negative effect on the main piston.

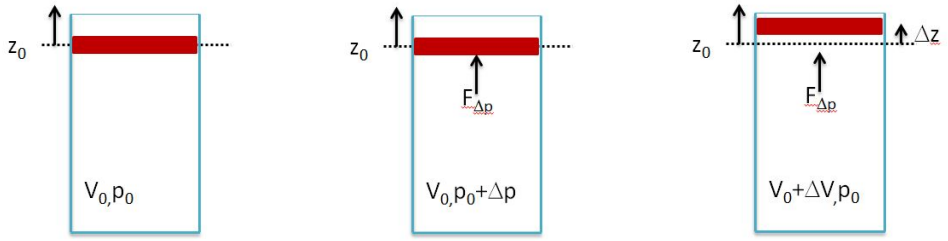

(a) Resting position

(b) Force acting on main piston

(c) Acceleration of the main piston

Figure 4.1: Working principle of a regular airpot: In the situation of figure 4.1a the airpot is in resting position. When a vibration is introduced, a pressure deviation will occur inside the pressurized volume, which will cause a force on the main piston (figure 4.1b). This force will accelerate this piston and move it to a new resting position such that the equilibrium at the main piston is obtained (figure 4.1c). This acceleration of the main piston is undesired.

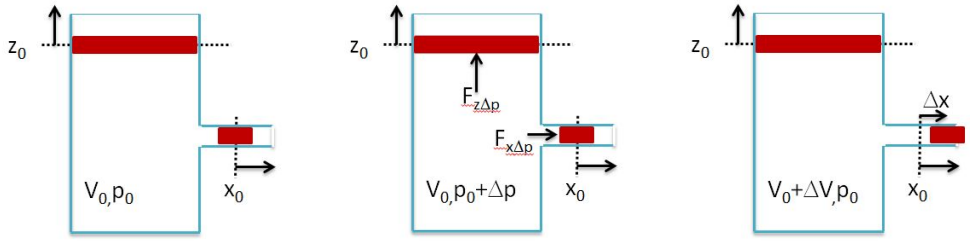

(a) Resting position

(b) Force acting on main- and add-on piston

(c) Acceleration of the add-on piston

Figure 4.2: Working principle of the airpot with add-on concept: The system is first in an equilibrium situation (figure 4.2a). Then a pressure deviation due to a ground vibration, causes a force exerted on both the main piston and the add-on piston (figure 4.2b). Due to its low mass the add-on reacts faster, resulting in a volume increase at the add-on, thus returning the pressure to its original state and therefore no additional force is acting on the main piston (figure 4.2c)

4.3 Formula derivation

In this section the derivation is shown of important formulas for airpots. This derivation was done to obtain a better understanding of the working principle and to not simply assume formulas found in literature. One of the results of doing this was that an often neglected term was discovered. This term is highlighted in red in equation 4.5. This term could be neglected if pressures inside the pot are far greater than the ambient pressure, however if the overpressure is not that large this term has a significant effect on the performance.

Spring stiffness

$$k_z = -\frac{rp_{in}A^2}{V} \tag{4.1}$$

Derivation The force is given by: $F = A \cdot (p_{in} - p_a)$ For the airpot, the area is constant; thus the force only changes with the pressure change, either inside or outside the pot. To determine the stiffness in z-direction, the derivative of the force is taken with respect to z; the change in ambient pressure due to a movement in z is 0.

$$k_z = \frac{dF}{dz} = \frac{d\left[A \cdot (p_{in} - p_a)\right]}{dz} = A\left(\frac{dp_{in}}{dz} - \frac{dp_a}{dz}\right) = A\frac{dp_{in}}{dz} \tag{4.2}$$

For the derivative of pressure to z, $pV^r = cst$ is used. The remaining term in equation 4.3: $\frac{dV}{dz}$ equals A (Volume is height times area). By rearranging the terms a formula for $\frac{dp}{dz}$ is obtained (equation 4.4). Substituting the result in equation 4.2 gives equation 4.1.

$$\frac{d(pV^r)}{dz} = 0 => \frac{dp}{dz}V^r + p\frac{dV^r}{dz} = \frac{dp}{dz}V^r + rpV^{r-1}\frac{dV}{dz} = 0 \tag{4.3}$$

$$\frac{dp}{dz} = -\frac{rpV^{r-1}\frac{dV}{dz}}{V^r} = -\frac{rpA}{V} \tag{4.4}$$

Natural frequency

$$f_n = \frac{1}{2\pi}\sqrt{\left(1 + \frac{p_a}{p_{in} - p_a}\right)\frac{rgA}{V}} \tag{4.5}$$

Derivation For the derivation of the formula for the natural frequency, the knowledge is used that the weight of the table and load is compensated by the force generated by the pressure inside the airpot. This means that these forces are in equilibrium: $F = m \cdot g = (p_{in} - p_a) \cdot A$. Hence we can rewrite this equation as: $\frac{A}{mg} = \frac{1}{p_{in} - p_a}$, which is used in equation 4.6.

$$\omega_n = \sqrt{\frac{k_z}{m}} = \sqrt{\frac{rp_{in}A^2}{Vm}} = \sqrt{\frac{p_{in}A}{mg}\frac{rAg}{V}} = \sqrt{\left(\frac{(p_{in} - p_a)\,A}{mg} + \frac{p_aA}{mg}\right)\frac{rAg}{V}} =$$
$$\sqrt{\left(\frac{(p_{in} - p_a)}{p_{in} - p_a} + \frac{p_a}{p_{in} - p_a}\right)\frac{rAg}{V}} = \sqrt{\left(1 + \frac{p_a}{p_{in} - p_a}\right)\frac{rAg}{V}} \tag{4.6}$$

4.4 Using magnetism for an ideal add-on

Magnets have the advantage that they have no mechanical damping or hysteresis. A magnetic setup with a comparable setup as Berkhof [5] could supply the required low/zero-stiffness behaviour, the moving magnet can act as the piston, which can be relatively low weight. To seal the airpot at the add-on, ferro-fluids can be used [6][7]. Thus the research by Berkhof is potentially a very good option to use as an add-on. Before designing a system we need to know what characteristics such a system should have to be useful for the add-on concept, which is why the model was required which is derived in chapter 5.

4.5 Atmospheric pressure variation

In the design and use of high precision devices all small changing factors should be taken into account, since small deviations can cause huge errors upon the performance of machines. One of these factors with small variation is the atmospheric pressure, which is not constant.

The ambient pressure has a diurnal variation due to radiational forcing which is dependent on the geological location (latitude) and varies from 0.3 mbar in the polar regions to 3 mbar at the tropics [8]. Besides these diurnal variations there are changes in the pressure due to the so called dynamic forcing, which has larger deviations in pressure, normally between 1000 and 1030 mbar with extreme recordings from 870 to 1086 mbar[9].

Chapter 5

Theoretical Model

5.1 Introduction

In this section a theoretical model is build for the proposed add-on concept for improving passive airpot vibration isolators. In section 5.2 the force equilibria are derived. These equilibria are the basis for the model to compute the transmissibility functions, which is covered in section 5.3. Using the found transmissibility function the potential performance in vibration isolation of the system is shown in section 5.4. In the last section of this chapter, section 5.5, the expected result for a model without add-on, but with added negative stiffness at the main piston is discussed. This result will be used in the validation of the obtained model.

5.2 Force equilibrium

In figure 5.1 the forces on the main- and add-on pistons are visualized. These forces can be subdivided into contributions of multiple factors. This is shown in equation 5.1. The system is in equilibrium if $F_1 = F_2$ and $F_3 = F_4$. The function $f(x_{add-on})$ is the force exerted by add-on which required to obtain the force equilibrium. These equilibrium equations are the basis for the mathematical relations used in the modelling of the add-on concept.

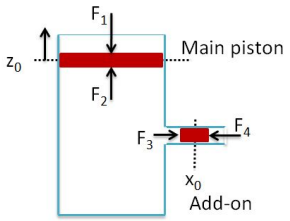

Figure 5.1: Overview of forces

$$
\begin{aligned}
F_1 &= F_{load} + F_{outsideair} = m_{load} \cdot g + A_{piston} \cdot p_{ambient} \\
F_2 &= F_{insideair1} = A_{piston} \cdot p_{airpot} \\
F_3 &= F_{insideair2} = A_{add-on} \cdot p_{airpot} \\
F_4 &= F_{addon} + F_{outsideair} = f(x_{add-on}) + A_{valve} \cdot p_{ambient}
\end{aligned} \tag{5.1}
$$

5.3 Transmissibility Function

Attempts to find transfer functions through computing the equations of motion based on free body diagrams did not work, and therefore an alternative was sought. This alternative was found in the "Signal Flow Graph Theory" [10]. First the block diagram in figure 5.3 was produced. This is by reasoning the different effects a disturbance, δ, would have on the different components discussed in section 4.2. The derivation of this block diagram is shown in figure 5.2. The three effects, namely the relative motion (A), the force on the main piston (B) and the force on the add-on pistons(C) are paths in the block diagram. Also if one of the pistons is moved, this will also cause a pressure deviation in the system, which will result in a force change on the other piston. This is the cause for the two return paths (a) and (b).

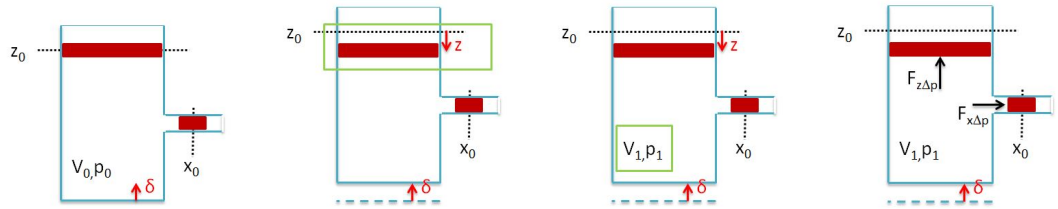

(a) Disturbance δ acts on the airpot frame (b) Relative movement main piston (c) Volume decrease and pressure increase (d) Additional forces on both pistons

Figure 5.2: The ground disturbance causes the airpot frame to move up (or down), this causes a relative motion between the main piston and the airpot frame, z, also due to the pressure increase additional forces act on the pistons.

From this block diagram a flow graph was drawn, which was then analysed using the Signal Flow Graph theory to compute the transmissibility functions, which are shown in figure 5.2 and 5.3. The used flow diagram is shown in figure 5.4. The derivation of these transfer functions is shown in appendix A.

$$
\frac{Z}{\delta} = \frac{A_g A_p \frac{p_0}{V_0} G_z - A_g A_p \left(A_a \frac{p_0}{V_0}\right)^2 G_x G_z + G_d G_z}{1 - \left(A_a A_p \frac{p_0}{V_0}\right)^2 G_x G_z} \tag{5.2}
$$

$$
\frac{X}{\delta} = \frac{A_g A_a \frac{p_0}{V_0} G_x - A_g A_a \left(A_p \frac{p_0}{V_0}\right)^2 G_x G_z - A_p A_a \frac{p_0}{V_0} G_d G_x G_z}{1 - \left(A_a A_p \frac{p_0}{V_0}\right)^2 G_x G_z} \tag{5.3}
$$

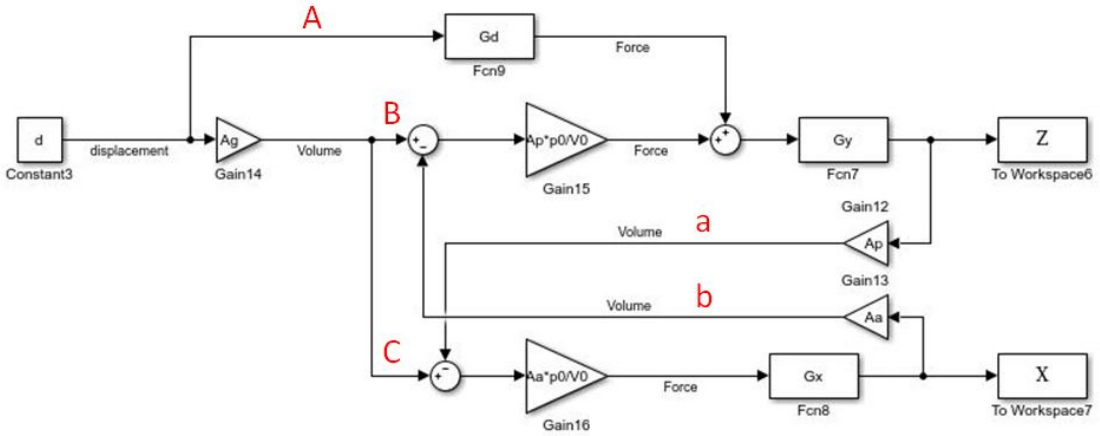

Figure 5.3: Block Diagram of interacting parameters. Gx, Gz and Gd are shown in equations 5.4 to 5.6

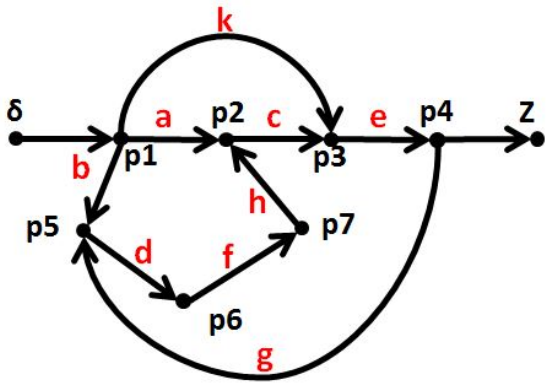

Figure 5.4: Flow Diagram of the system including the add-on. Node p7 is the movement of the piston in X-direction.

$$Gz = \frac{1}{M_t s^2 + cz_t s + kz_t} \tag{5.4}$$

$$Gx = \frac{1}{m_t s^2 + cx_t s + kx_t} \tag{5.5}$$

$$Gd = \frac{\frac{Ag}{Ap} cz_t s + \frac{Ag}{Ap} kz_a}{1} \tag{5.6}$$

5.4 Modelled results of the system with add-on

By the derivation of the transfer functions in 5.3 a model is created. Using this model the parameters can be tuned such that a desired transmissibility curve is obtained. In appendix C the effect of the different parameters on the full system is visualized. Figure 5.5 shows the

response of an airpot system with incorporated add-on, as derived by the model. The low frequency phase lead of *With Add-on: X* is discussed in section 5.4.1.

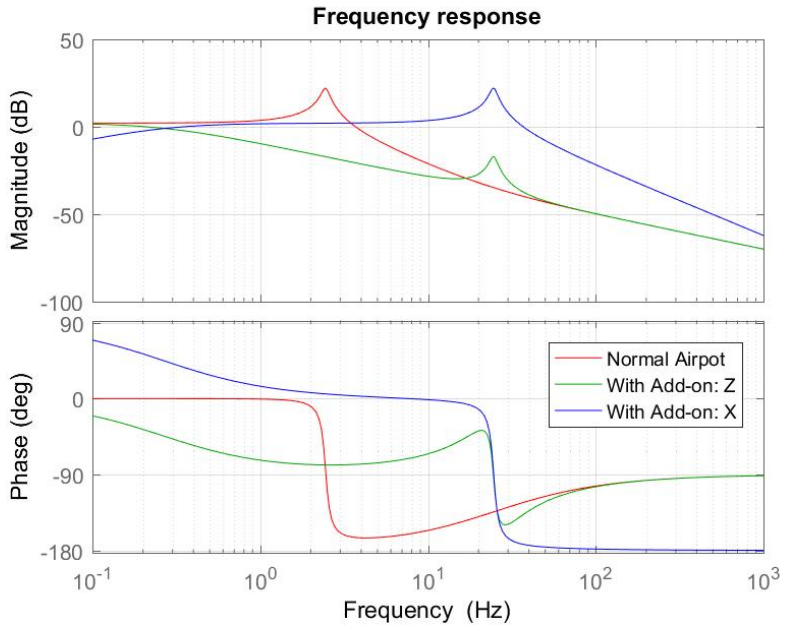

Figure 5.5: In this graph the performance potential of the concept with add-on is shown. The green line represents the response of the main piston, which should have a minimal response to an input disturbance. The blue line shows the response of the add-on.
($m = 0.1\,\text{kg}, D_a = D_p = 0.08\,\text{m}, D_g = 0.09\,\text{m}, \zeta = 0.05$.)

In figure 5.5 we can see that the transmissibility from a ground disturbance to the load-carrying piston is indeed reduced in the 1-10 Hz range, which previously showed the undesired peak. (Section 3.2.1) However we can see that at a higher frequency the transmissibility is larger than the original system, in this case at $\approx 15 - 60\,\text{Hz}$, this is not desirable. This downside of the add-on concept should be taken into account when deciding if this system is suited for a specific application. If additional damping is added to the piston (increasing $\zeta > 0.05$), this negative effect can be reduced, however this also reduces the vibration isolation gain in the 1-10 Hz range (Figure 5.6).

5.4.1 Remarks on the model

In modelling this concept, some assumptions and simplifications were made. Due to limitations in the signal flow graph model, the adiabatic index of air (r = 1.4) which is present in the formulas of pneumatic vibration isolators (equations 4.1 and 4.5) is not taken into account, therefore it is expected that the frequency of the resonance peak of the modelled transmissibility will be a factor $\sqrt{1.4} \approx 1.2$ lower than the measured resonance frequency. Also pressure deviations are taken to be uniform over the volume, the speed of travelling pressure waves is not incorporated in the model.

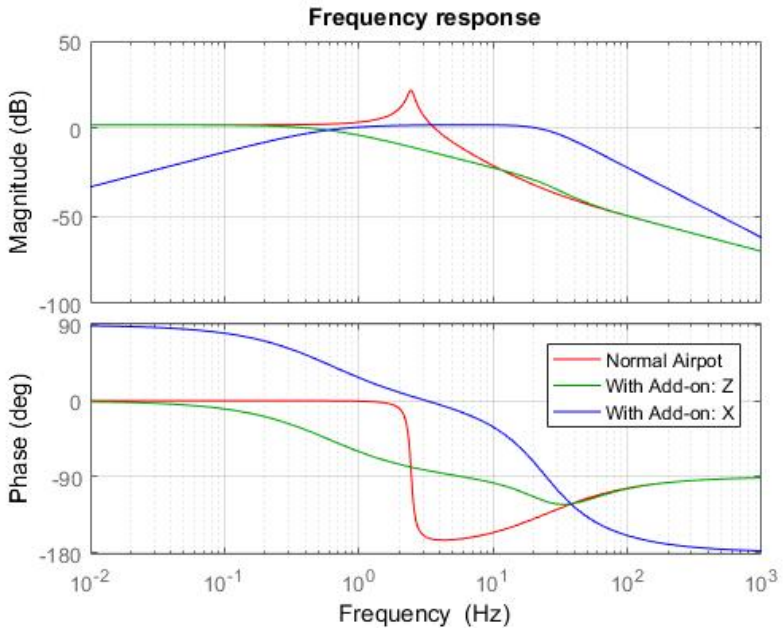

Figure 5.6: Reducing the negative effect at higher frequency (compared to 5.5. The peak in the $\approx 15 - 60\,\text{Hz}$ range is reduced, but at the cost of reducing the isolation improvement in the 1-10 Hz range. ($m = 0.1\,\text{kg}, D_a = D_p = 0.08\,\text{m}, D_g = 0.09\,\text{m}, \zeta = 0.05, ca_x = 20\,\text{Ns/m}$.)

This potential performance plot is created with parameters that are tuned without any optimization, therefore it is expected that a better performance is possible than the performance discussed in section 5.4. The optimization has not been done since the model is not validated yet, if the model would deviate from reality the optimization would not result in optimal performance. Hence validation was given priority.

As described in figure 5.5, there is unexpected behaviour in the low frequency range ($< 0.1\,\text{Hz}$). After investigation this is most likely caused by round-off errors in the calculation of the transmissibility functions. The effect is shown in figure 5.7.

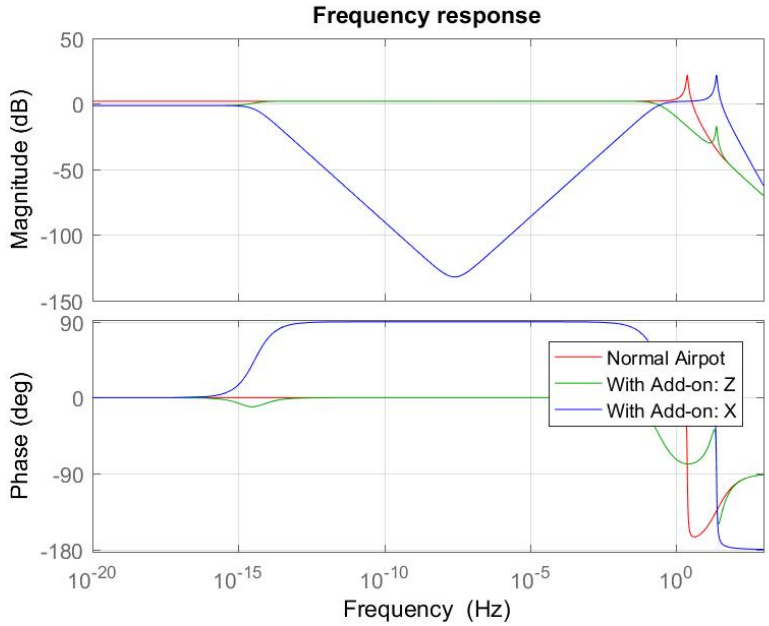

Figure 5.7: Unexpected low frequency effects in the mode, most likely caused by round-off errors as discussed in section 5.4.1. ($m = 0.1\,\mathrm{kg}, D_a = D_p = 0.08\,\mathrm{m}, D_g = 0.09\,\mathrm{m}, \zeta = 0.05$)

5.5 Addition of negative stiffness at main piston

Due to time limitations, not the entire model is validated. It was estimated that a full design and fabrication of an add-on with the characteristics as used in the modelling of section 5.4 could be a research thesis on itself, especially if the benefits of magnetic systems was to be exploited (section 4.4. To verify part of the theoretical model but also to show that an airpot can be made in-house at the PME-department of Mechanical Engineering at the TU-Delft, it was decided to build a demonstrator (Chapter 6) with negative stiffness added at the piston (comparable to the minus-K solution discussed in section 3.2.2.)

In figure 5.8 the stiffness and forces as a function of vertical piston displacement are shown of the three sub-systems. (The load (F_z), pressurized airpot (F_p) and the negative spring setup (F_{ns}) as well their summation). As can be seen in the figure, the negative stiffness value is only valid in exactly the operating point. If the system is not working at this operating point, the effect of the spring configuration is greatly diminished. To overcome this problem a theoretical solution was designed and calculated, which is shown in appendix B.5. In the case that due to the added negative stiffness the total stiffness of the main piston is reduced with 99%, a significant shift in the frequency of the resonance peak is expected. (Figure 5.9).

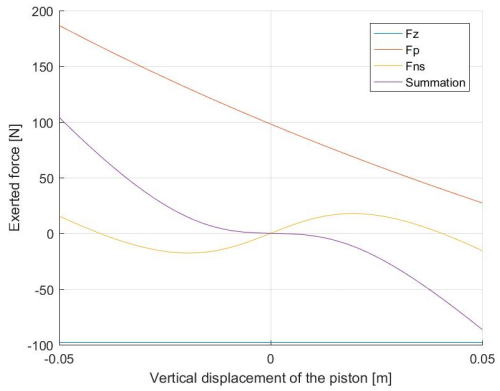

(a) The forces of the different sub-systems and their combination

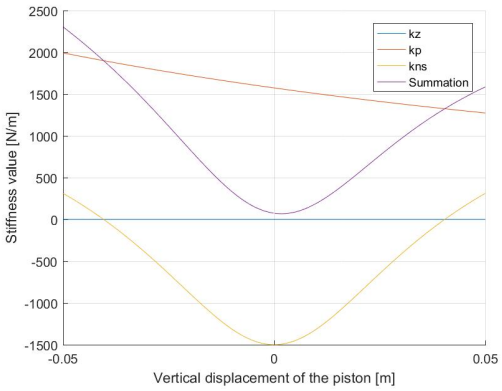

(b) The stiffness effects of the different sub-systems and their combination

Figure 5.8: In these two figures the force and stiffness values acting on the main piston are shown. Observe the almost zero stiffness value at the operating point (vertical displacement is zero).($M = 10\,\mathrm{kg}, D_p = 0.08\,\mathrm{m}, D_g = 0.09\,\mathrm{m}, L_0 = 0.0508\,\mathrm{m}, L_p = 0.02\,\mathrm{m}, k_s = 770\,\mathrm{N/m}$)

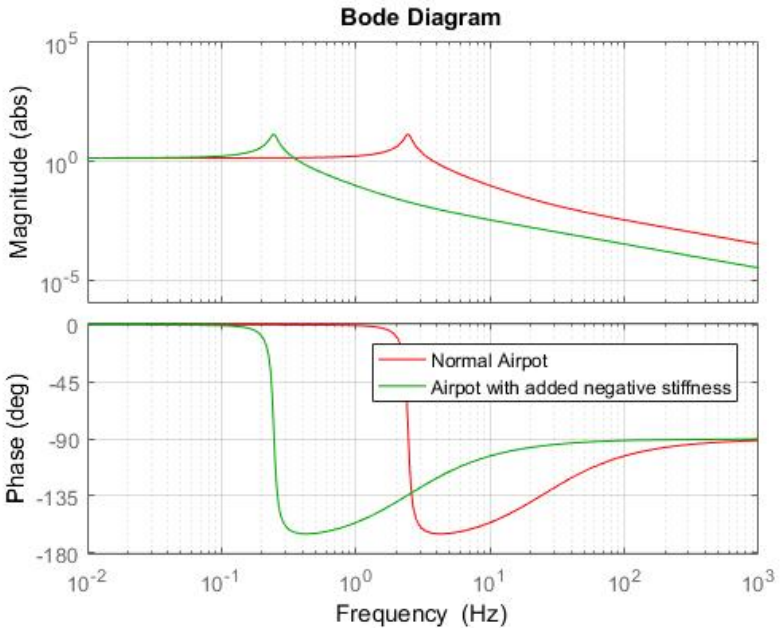

Figure 5.9: Change in frequency response

5.6 Conclusions

A model was build using Signal Flow Graph theory for the system with the add-on concept. According to this model the concept is potentially a very good isolator for the lower frequencies. However it comes at a cost that there is a frequency range above the resonance frequency where the system will perform worse than the original airpot 5.4. Due to time limitations the demonstrator will not have an incorporated add-on. Therefore it was decided to design a configuration which applies a negative stiffness to the main system, which can be used to validate part of the obtained model.

Chapter 6

Demonstrator to validate model

6.1 Introduction

In this chapter first the full design of the demonstrator is discussed (Section 6.2), followed by the measurement plan (Section 6.3) and the results (Section 6.4). The design in SolidWorks is shown in appendix E. The goal of this chapter is to step by step go through the working principle of the demonstrator, discuss its pro's and con's and show how the measurements are then used to validate the theoretical model of chapter 5.

6.2 Design

The full system is shown in figure 6.1. The setup is can be divided in certain sub-systems, based on the function that they add towards the whole system. These subsystems are: the frame, pressure seal, load, stoppers, the negative stiffness spring configuration, pressure supply and the measurement base. The measurement system is discussed in section 6.3.

6.2.1 Frame

The frame of this demonstrator should be airtight up to 1.5 bar, in that case loads up to 20 kg can be applied. For the frame a T-section of PVC pipe is chosen (figure 6.2b), since it can withstand the pressure and has the possibility to mount an additional piston (the add-on) at the "T". (Figure 6.2b)

6.2.2 Pressure-seal

There are multiple ways of sealing the airpot while remaining a certain allowance for movement around the piston, for instance a rolling diaphragms [11] or ferrofluid seals [6][7]. For this demonstrator a rubber band used in a subwoofer, as shown in figure 6.2a, is used, which is technically a limited stroke rolling diaphragm.

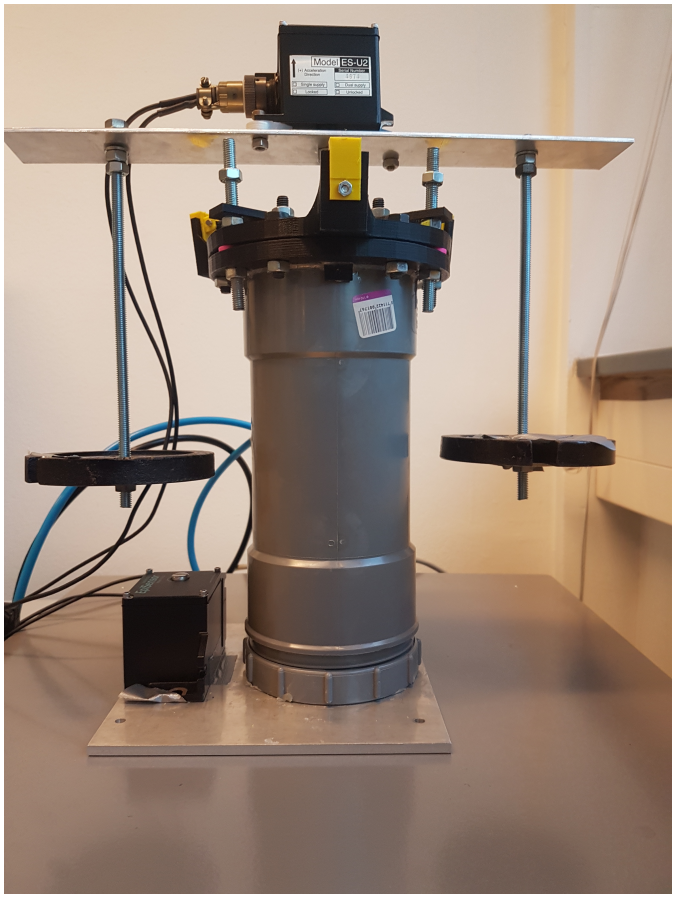

Figure 6.1: Image of the demonstrator including the measurement tools. The T-section of the frame, described in 6.2.1, is at the backside. The connection to the pressuresupply is connected at the T-section, described in 6.2.1, which is located at the other side of the setup.

6.2.3 Load

In normal applications, a table used for high precision images is supported by at least four table legs with build-in airpots. Since only one demonstrator is build for this thesis, balancing was expected to become an issue. Therefore it is chosen to have a crossbeam with masses at both ends, the centre of gravity of this mass is below the rotational point of the piston, balancing the system for tilts around the x- and y-axis. This subsystem is designed such that masses can be added and removed easily to allow mass variation for the measurements.

6.2.4 Negative Stiffness

To provide the negative stiffness, a spring configuration is used which is described in section 5.5. Springs available in the Mechatronicslab at PME were used ($L_0 = 0.0595\,\mathrm{m}, k = 960\,\mathrm{N/m}, L_p = 0.017\,\mathrm{m}$). Which allowed for a maximum negative stiffness application of $1154\,\mathrm{N/m}$. In the design some tuneability options are present. The height relative to the piston can be changed

(a) Rubber band.

(b) T-section PVC pipe

Figure 6.2: Used off-the-shelf parts.

by the slots in the upper part of the frame. The tensioning of the springs can be changed by turning the spring-holder, with tapped M4 thread, over the M4 bolt. Also to keep the force on the piston acting in-line with the springs, the springs were added to the frame using a rotational joint 6.3.

6.2.5 Stoppers

The setup is equipped with stoppers for safety concerns, the movement of the piston is restricted in vertical direction (both up and down) as well as for small rotational forces) around the z-axis and for in-plane movements. This is done by three stoppers, placed 120° apart from each on the piston. They are connected to the frame using a M8 bolt-hole combination. The in-plane and rotation about the z-axis are limited with a fixed value, the vertical range can be adjusted by the M8 nuts. The realisation of these stoppers is shown in figure 6.3.

6.2.6 Pressure supply

The pressure supply was present at the mechatronics lab, which was equipped with a control knob which allowed for a rough setting on the supplied pressure. This pressure outlet was connected to a connection block. Figure 6.4 A valve is placed between the supply and this connection block (D), other connection are A) a pressure sensor (see section 6.3.2), B) an outlet to allow the release of pressure from the system and C) a connection to the airpot.

6.2.7 Base

To have a common ground for both the airpot and the reference accelerometer a steel plate was used to mount them both on, for fixation bee-wax is used.

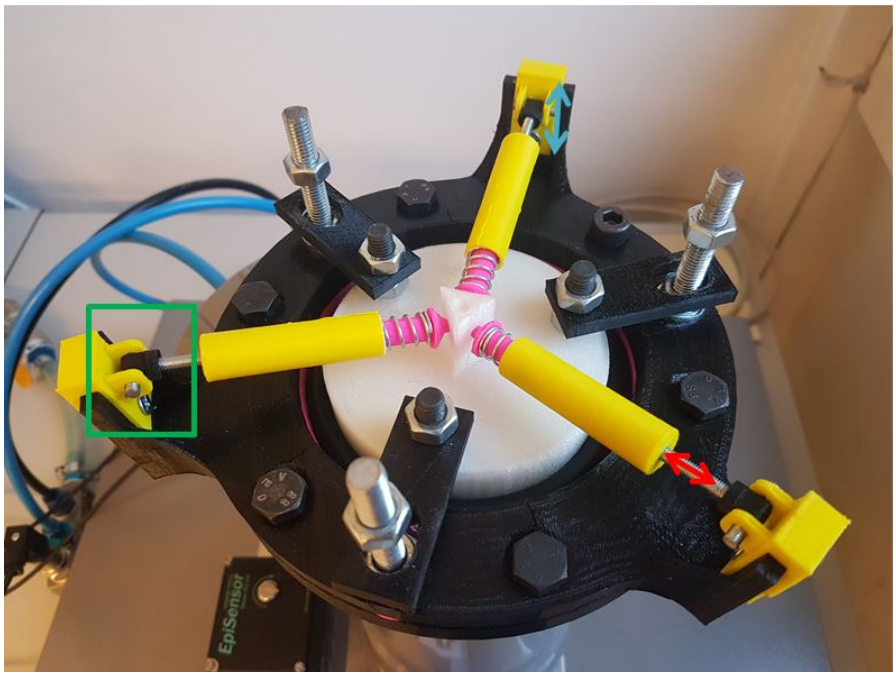

Figure 6.3: Spring configuration and stoppers. In this figure the adjustability of height (blue arrow) and the pre-tensioning (red arrow) are indicated as well as the rotational joint (green box). Also the installed stoppers are shown.

6.3 Measurement setup

6.3.1 Combining different measurements

The available shaker was not strong enough to apply a large enough amplitude for frequencies below < 5 Hz (as can be seen in figure 6.10b), hence it was not possible to actuate with a controlled frequency and amplitude. To circumvent this problem, two accelerometers were used, one to measure the input vibration and one to measure the vibrations on top of the airpot. The ratio of the Fast Fourier Transforms (FFT) of both accelerometers will provided the transmissibility curve that is a performance measure for the isolation capabilities of a vibration isolator (as discussed in section 3.1.2).

6.3.2 Sensors

For the measurements 3 sensors are used. Two *EpiSensor* force balance accelerometers (Model FBA ES-U2) [12] and a *Gems* pressure sensor (Model 3500B02B5G01B00RS) [13]. These are connected to a laptop using a *National Instruments* data acquisition box (NI USB-6008) [14]. The two accelerometers are powered by a *Delta Elektronica* power supply (Model ES 030-5), the pressure sensor by a standard 12 V adapter and the acquisition box through the USB connection with the laptop.

(a) Tuneability of pressure supply

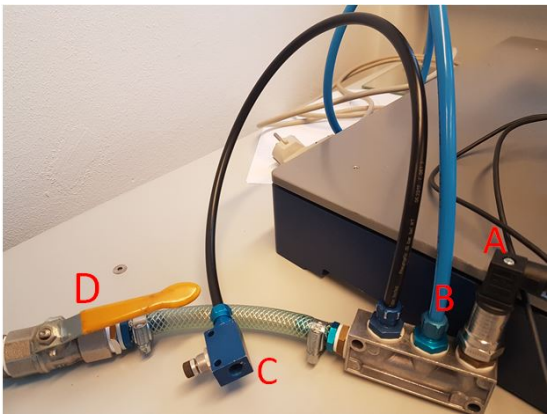

(b) Connection block pressure supply

Figure 6.4: Functionalities and connections of the pressure supply

6.3.3 Data Analysis

The collected data was read using LabView. The measurements could be tracked live to see if everything was functioning correctly, the interface is shown in figure 6.6a. The LabView block diagram was created using the help of Jos van Driel, who works as Lab Assistant at the 3mE "meetshop", a facility where measurement equipment can be obtained for research done at the Delft University of Technology. The program writes the measurements into a text file (.txt) which can be used by Matlab to import the obtained data.

From the acceleration data a Frequency Response Function (FRF) is computed. This is done by dividing the auto spectral density of the output by the cross spectral density of the input and output. (Equation 6.1)

$$H = \frac{\text{Auto Spectral Density of Output}}{\text{Cross Spectral Density of input and Output}} = \frac{Szz}{Sxz} \tag{6.1}$$

6.3.4 Actuator

An improvised shaker was used as shown in figure 6.7. It has a mass that is actuated using an old loudspeaker and linear guidance is used to keep the movement in one directional. This loudspeaker was actuated using a control unit from Ling Dynamic Systems (Model TP0-20) which allowed manual tuning of the amplitude and the frequency.

6.3.5 Base

To check if the steel plate would be a good base for this system, a measurement was done with the two accelerometers placed on this base and to see that they yield the same response (transmissibility = 1) when vibrations were introduced. This intermediate setup is shown in 6.8.

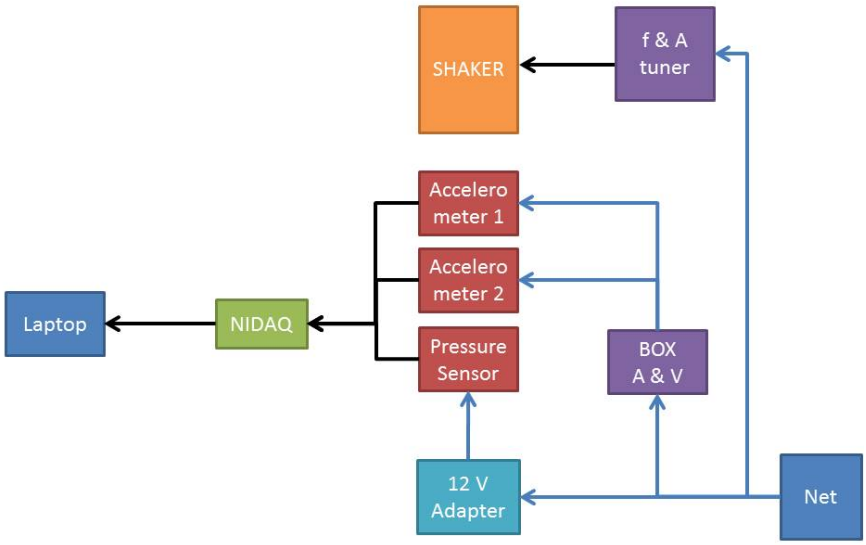

Figure 6.5: Schematic overview of the measurement setup.

In figure 6.9 we can see that there is indeed a good 1-on-1 transmissibility in the $\approx 1 - 60\,\mathrm{Hz}$ range. This base was then placed on a low stiffness table, such that the self-actuation could be done more easily.

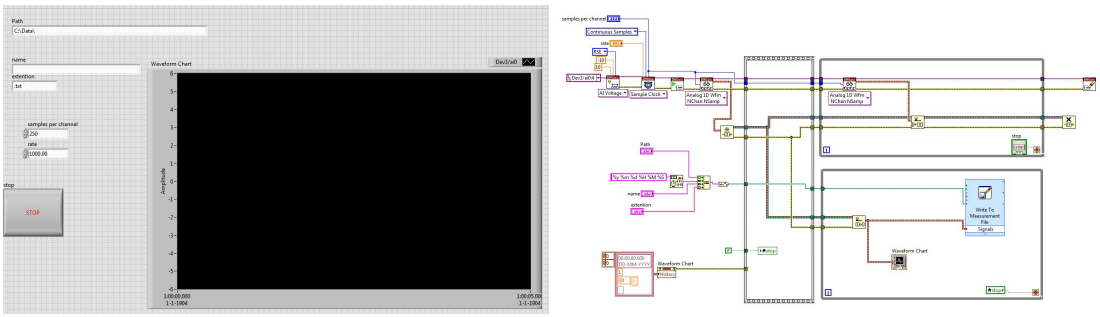

(a) LabViewLive. (b) LabView Data Collection.

Figure 6.6: LabView

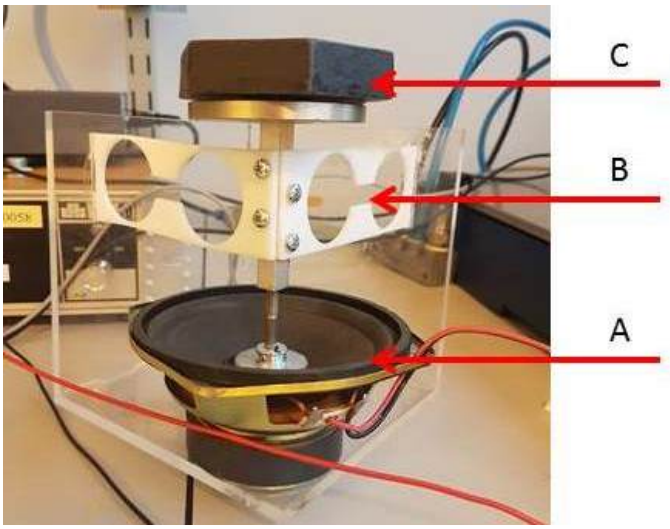

Figure 6.7: The shaker used for actuation. It consists of 3 main parts: A) a loudspeaker, B) linear guidance and C) added weight.

Figure 6.8: Measurement check to confirm equal input signals.

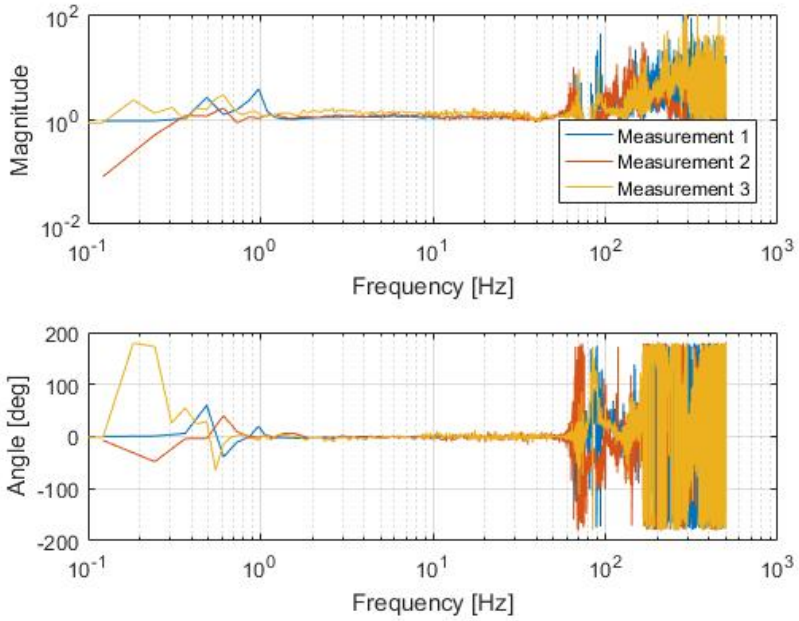

Figure 6.9: Measurement check to confirm validity to use the steel plate as a base.

6.4 Initial results

In figure 6.10 it can be seen that a transmissibility plot is obtained which shows a trend comparable with the airpot performances found in literature (section 3.2.1). We can see that the self-actuated measurement (in figure 6.10a) shows a smooth response in the lower frequency range (0.5-10 Hz), and the shaker actuated measurement in the 5-20 Hz range. In chapter 7 the results are analysed in more detail and compared with the expected results from the model.

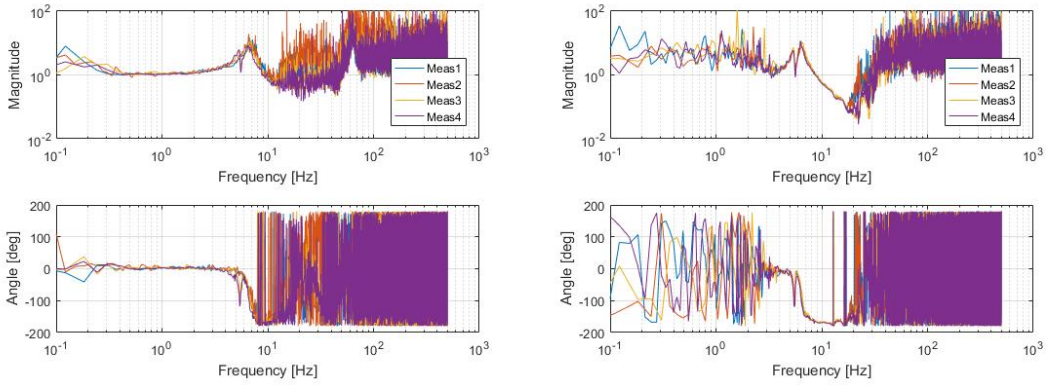

(a) Measurement results with a load mass of 2 kg, self actuated (low frequency)

(b) Measurement results with a load mass of 2 kg, actuated with the shaker

Figure 6.10: Initial measurement results

6.4.1 Remarks

One of the main issues of building this demonstrator proved to be the sealing of this airpot. Leakage was quite significant and a constant (pressurized-)air supply was needed to prevent the piston and the load to fall upon the lower vertical limit of the system. This will have an influence on the performance of the airpot, but also is a deviation with respect to the model. One of the main causes of this leakage was the use of 3D-printed parts, this allowed great freedom in the design, but it was not managed to print these parts airtight, even though this should be possible. Coating with glue helped to reduce the leakage flow but did not stop it entirely.

Though the self actuation provided the means to analyse the lower frequency range, it is far from ideal as the repeatability of such a measurement is debatable.

In trying to prevent, or at least reducing the leakage, some additional parts were created which are shown in appendix E. Also by tightening the bolts too fast for this purpose parts of the model started to deform, which was visually determined. Which resulted in changes in distances between parts, this is further discussed in section 7.2.2.

6.5 Conclusions

A demonstrator was build using off the shelf and 3D printed parts. This demonstrator is a working vibration isolation airpot, however the leakage is so significant that it requires a constant pressurized air-supply. Though a suited shaker was not available, using some smart tricks measurements were done over the entire range of interest. The data was analysed using LabView and Matlab. Even though there is quite some room for improvement of this demonstrator, it can be used for initial verification of the model.

Chapter 7

Validation of concept model

7.1 Introduction

In this section the realized model, chapter 5, is compared with the measurement results of the demonstrator, section 6. The performance of the demonstrator as a normal airpot is discussed in section 7.2. In sections 7.2.1 and 7.2.2 the measurements of specific parameters, mass and negative stiffness, are discussed.

7.2 Measurements

As mentioned in section 6.4 the general trend of the measurements was comparable with that of the airpots found in literature. (Shown in section 3.2.1) In figure 7.1 the expected (modelled) response of the airpot is shown, as well as the measurement averages from both the self-actuated measurements and those obtained with the shaker. Large discrepancies between model and measurements are observed in both the frequency of the resonance peak and in the gain at low frequencies.

After investigation it was found out that one of the reasons for this discrepancy was a wrong assumption in the parameters of the model. The parameter D_p was taken to be the diameter of the piston. However the rubber band used in the design, section 6.2.2, has a relatively large surface area on which the pressure also exerts a force. This is visualized in figure 7.2. When the parameter is changed according to this realisation, figure 7.3 is obtained. Still a deviation is present in the resonance frequency, this can however be explained by the fact that the compressibility of air (n=1.4) is neglected in the model as described in section 5.4.1. Hence the resonance frequency in reality is expected to be a factor $\sqrt{(}1.4) \approx 1.2$ higher than the modelled result, which then matches that of the measurements.

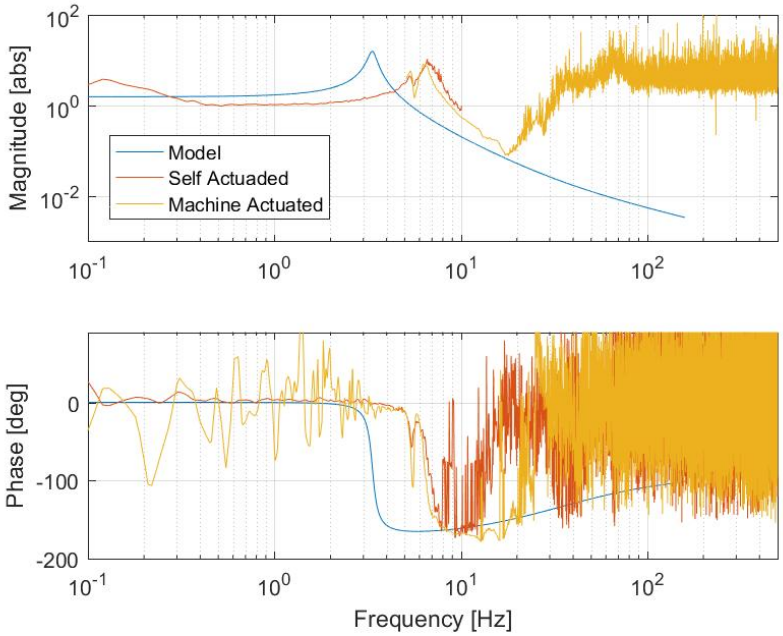

Figure 7.1: In this figure the model and the measurement results are shown. It can be observed that there is quite a large discrepancy between the measured data and the model, the eigenfrequency of the model is at $\approx 3.4\,\text{Hz}$ while those of the measured data is at $\approx 6.5\,\text{Hz}$. (Parameters for the model $M = 2\,\text{kg}, D_g = 0.11\,\text{m}, D_p = 0.088\,\text{m}$)

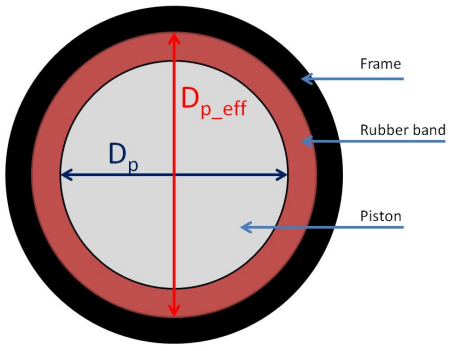

Figure 7.2: Bottom view of the piston and the rubber band of the demonstrator. This figure shows the difference between the area of the piston (based on D_p) and the total, larger, effective area (based on D_{p_eff})

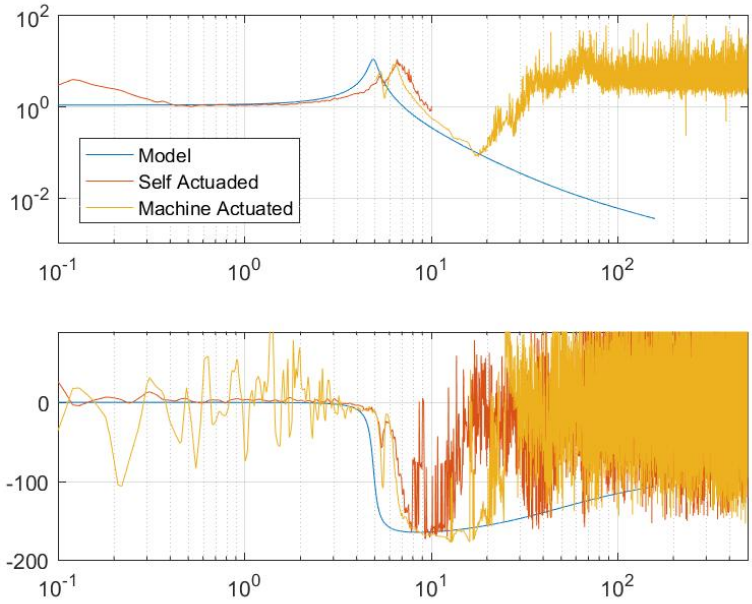

Figure 7.3: The effective area of the piston was adjusted (as compared to figure 7.1) and the model and measurement show a better comparison. (Parameters for the model $M = 2\,\mathrm{kg}, D_g = 0.11\,\mathrm{m}, D_p = 0.107\,\mathrm{m}$)

7.2.1 Mass variation

After this first analysis a similar measurement was done with the only difference that the added mass was increased from 2 kg to 6 kg. The result is shown in figure 7.4. Here we can see that the resonance-peak in the model is shifted to a lower frequency as was expected according to equation 4.5, though the resonance frequency of the measurement results is shifted minimally. When the average pressure is taken from the measurement something interesting can be seen. The average overpressure in the case that the added mass is 2 kg an overpressure of 1.045 bar is measured, according to $Mg = pA_p$ ($D_p = 0.107$ m) this corresponds to load capability of 4.38 kg. If the same thing is done for the 6 kg a load capability of 4.65 kg is obtained. Clearly this cannot be correct since the system was capable of lifting the added 6 kg. Most likely leakage might be the cause of these unexpected values: as mentioned in section 6.4.1 a continuous flow from the pressure-supply to the airpot is present to maintain the required pressure in the airpot. Since the pressure is therefore not static, flow effects most likely change the response of the pressure sensor.

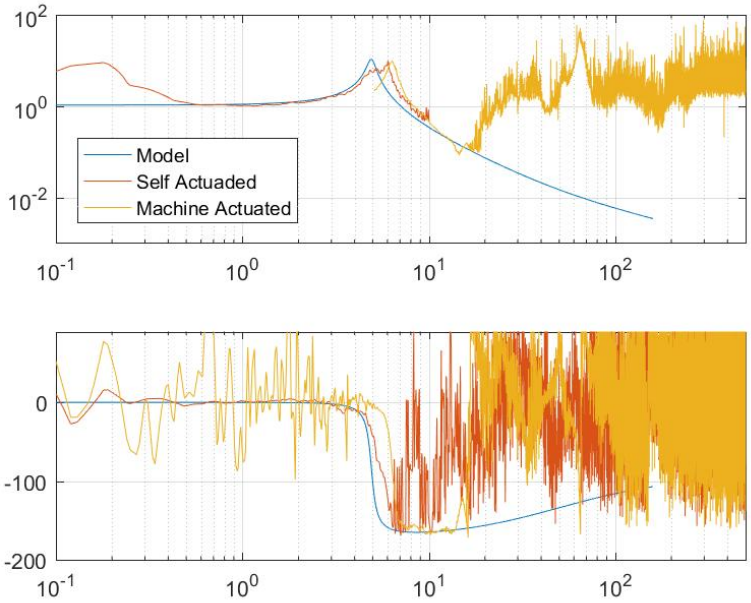

Figure 7.4: Result of the model and the measurements for a larger mass.
($M = 6$ kg, $D_g = 0.11$ m, $D_p = 0.107$ m)

7.2.2 Adding negative stiffness

According to the model of section 5.5 and the springs described in section 6.2.4 the response in figure 7.5 is expected. Measurements have been done to verify this. The result is shown in figure 7.6. Instead of the expected shift to the left, a (very) small shift to the right can be observed. After obtaining this result the demonstrator was inspected to check for potential causes, deformations due to over-tightening of the bolts in attempts to reduce the leakage were found. This

comprises the alignment of the spring configuration, which could explain the difference.

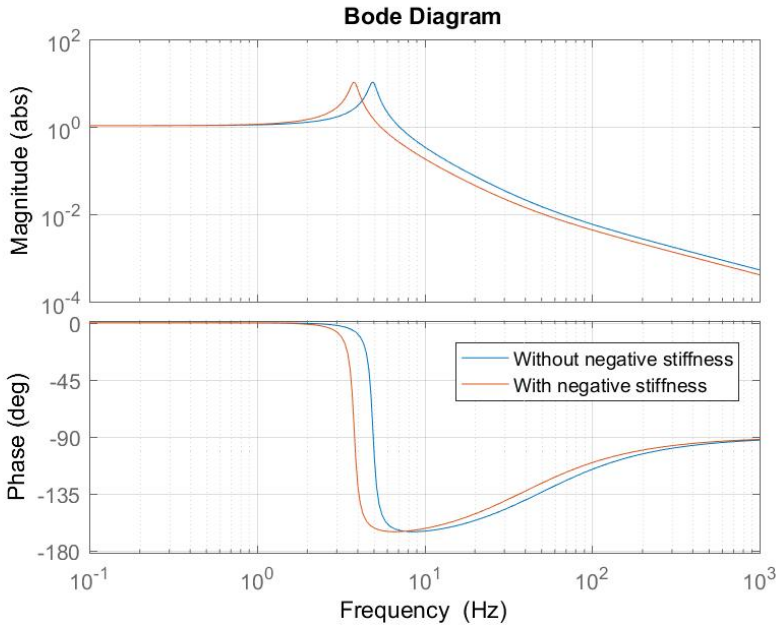

Figure 7.5: Expected effect of the negative stiffness on the demonstrator.($M = 2\,\mathrm{kg}, D_g = 0.11\,\mathrm{m}, D_p = 0.107\,\mathrm{m}, L_0 = 0.0595\,\mathrm{m}, L_p = 0.017\,\mathrm{m}, k_s = 960\,\mathrm{N/m}$)

7.3 Conclusions

Measurements of the demonstrator show that it performs successfully as a vibration isolator. Modelled trends however were not always matched. Increasing the mass yielded unexpected values especially for the pressure. These unexpected results are caused by the leakage of the system, which resulted in the need for a permanent pressurized air supply to maintain the required pressure for lifting the load placed on the demonstrator. Also the addition of negative stiffness did not have the intended, modelled, effect, most likely due to the deformations caused by attempts to reduce the leakage. Availability of a more reliable shaker will also help to obtain a more precise measurement result.

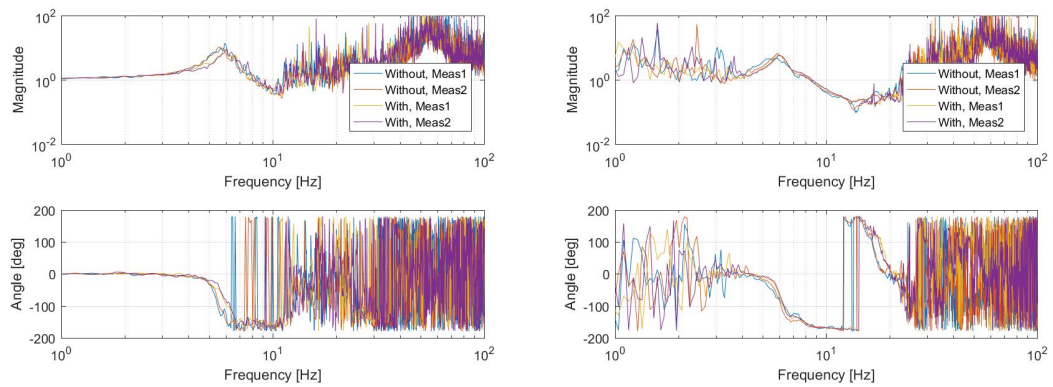

(a) Measurement results with a load mass of 2 kg, self actuated

(b) Measurement results with a load mass of 2 kg, actuated with the shaker

Figure 7.6: Measurement results of the system with and without added negative stiffness. "Without" and "With" indicates if the negative stiffness was applied or not. A very small difference can be seen between the two types of measurements, where the peak of the negative stiffness measurement is shifted slightly to the right.
($M = 2\,\mathrm{kg}, D_g = 0.11\,\mathrm{m}, D_p = 0.107\,\mathrm{m}, L_0 = 0.0595\,\mathrm{m}, L_p = 0.017\,\mathrm{m}, k_s = 960\,\mathrm{N/m}$)

Chapter 8

Conclusions and recommendations

As was stated in the introduction, the aim of this research was to investigate the potential of the (magnetic-) add-on concept when applied on existing pneumatic vibration isolation solutions, also known as "airpots". Objectives were to model this system, design and implement the add-on and verify the concept by means of building a demonstrator. This chapter presents the overall conclusions, as well as some recommendations for future research related to this novel concept.

8.1 Conclusions

Research was done in the state of the art in the field of vibration isolation. It was shown that there are quite some different solutions in the vibration isolation category, however most higher-end system require active control. Research was done to investigate if the proposed concept was already mentioned or implemented, no record of this was found and therefore it was decided to continue the research into the effect of using such an add-on on existing airpots.

Modelling of a multiple-piston airpot proved to be troublesome using the conventional methods, a solution was found using *Signal Flow Graph* theory. [10] This theory was the bases of the analytical model used to show the potential of the system. The results of the model show that the concept has indeed a large potential in the frequency range where normal airpots are lacking, however with the parameters used in this thesis there is a trade-off because the improvement around the original eigenfrequency comes at the cost of a small frequency range above the eigenfrequency where transmissibility is worse then with the standard airpot.

A test setup was build with the purpose of both validating the model and act as a functioning demonstrator to show prove-of-concept. Due to time limitations this test setup was not yet equipped with the proposed add-on, but with a spring configuration capable of adding negative stiffness to the main piston, which should also increase vibration isolation performance. [15] This spring configuration was, opposed to the add-on, deemed to be realizable in the time frame of this thesis. Since the model is also supposed to be able to cope with this regarding expected performance, this test setup is used to validate the model.

Since there was no accessibility to a high-end shaker, some creative techniques were used. A combination of methods was used to obtain measurement results for the required spectrum in the frequency domain. Measurements consisted of low-frequency human-actuated vibration measurements and higher-frequency measurements using a loudspeaker with linear guiding and added mass for actuation. These measurement results were combined and could successfully be compared with the analytical model.

The measurements show that the demonstrator is a functioning vibration isolator. It was tested up to an added load of 6 kg and showed to a certain extend results expected from the analytical model. However there were some discrepancies between the analytical model and the measurement results, namely that the spring configuration did not lower the eigenfrequency as was expected, this is caused by alignment errors in the final demonstrator. And the measurement results show other behaviour with variation in load than is expected, which is caused by the leakage of the system.

With the fabrication of this test setup some challenges arose concerning the airtightness of the system. One of the issues was the surface roughness was too high to seal the airpot using the clamped rubber band. Also leakage was present through some of the parts. Both issues can be allotted to the use of 3D-printed parts. Adjustments have been done to the clamping design of the rubber band, and the 3D-printed parts were coated with a layer of glue, though the leakage was reduced it was not completely eliminated. In attempts to reduce this effect deformations occurred to the design which caused the spring configuration not to have the desired effect.

Despite these issues the setup was tested for masses up to 6 kg and was shown to work as a functioning vibration isolator. Vibration isolation was obtained from a frequency of approximately 9 Hz (depending on the load). for frequencies above approximately 9 Hz (depending on the load). The measurement results indicated that the setup worked, to a certain extend, as was predicted by the realised model.

8.2 Recommendations

Since it was eventually left out of the scope of the research the add-on itself has to be designed and attached to either the demonstrator or an existing airpot as to verify the full analytical model and prove that it is indeed a valid passive vibration isolation solution. I would recommend to do this on an existing (commercial) airpot, since it would circumvent many fabrication issues which should not be the focus of the continued work. A collaboration with a company that produces airpots would greatly assist in keeping the focus on the add-on concept and its performance.

If a commercial airpot is not available, the test setup of this thesis can be used, however it is strongly recommended to substitute the PLA 3D-printed parts with a more suitable material.

Bibliography

[1] P. Chen and M. Shih, "Modeling and Robust Active Control of a Pneumatic Vibration Isolator," *Journal of Vibration and Control*, vol. 13, no. 11, pp. 1553–1571, 2007. [Online]. Available: http://jvc.sagepub.com/cgi/content/abstract/13/11/1553

[2] Lawrence Berkeley National Laboratory, "Precision Mechanisms," 2014. [Online]. Available: http://engineering.lbl.gov/precision-mechanisms/

[3] C. Crede and J. Ruzicka, "Theory of vibration isolation," *Shock and vibration handbook*, pp. 1–43, 1996.

[4] TMC, "General Introduction Vibration Isolation." [Online]. Available: http://www.techmfg.com/techinfo/technicalbackgroundindex/generalintroduction

[5] R. Berkhof, i. J. Spronck, and P. d. i. J. Herder, "Vertical vibration isolation using permanent magnets," 2015.

[6] G. Bakker, E. Blomme, B. Elders, and R. Haan, "Design of a dynamic cylindrical pressure controller with ferrofluid seal," Technical University Delft, Tech. Rep., 2016.

[7] Ferrotec, "Technology - Ferrofluidic Seals." [Online]. Available: https://seals.ferrotec.com/technology/

[8] F. Le Blancq, "Diurnal pressure variation: The atmospheric tide," *Weather*, 2011.

[9] J. Haby, "AIR PRESSURE ON WEATHERCASTS." [Online]. Available: http://www.theweatherprediction.com/habyhints2/410/

[10] S. J. Mason, "Feedback Theory - Some Properties of Signal Flow Graphs," *Proc. IRE*, vol. 41, no. 9, pp. 1144–1156, 1953.

[11] DiaCom Corporation, "Rolling Diaphragm Theory - Engineering and Design." [Online]. Available: http://www.diacom.com/rolling-diaphragm-theory

[12] EpiSensor, "Force Balance Accelerometer, Model FBA ES-U2 User Guide," 2005.

[13] Gems, "3500 Series Data Sheet," Tech. Rep.

[14] N. Instruments, "User Guide NI USB-6008/6009," Tech. Rep., 2015.

[15] D. L. Platus and J. McMahon, "Negative-Stiffness Vibration Isolation Gains Popularity," 2009. [Online]. Available: https://www.photonics.com/Article.aspx?AID=38385

Appendix A

Signal Flow Graph Derivation

A.1 Introduction

In this appendix the derivation and application of the signal flow graph theory is shown step by step, with the results the transfer functions that are used in the thesis work.

A.2 Step-by-step derivation

As described in section 5.3 Signal Flow Graph theory is used to compute the transfer-functions[10]. The block diagram A.1 is transformed into a signal flow graph **??**, for which the gains of the system are shown in table A.1.

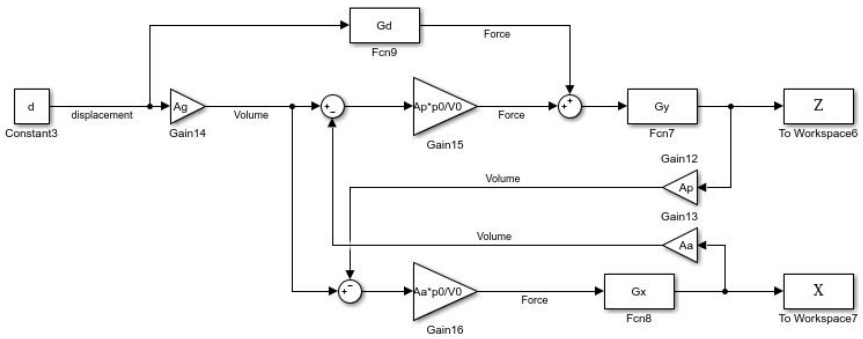

Figure A.1: Block Diagram of interacting parameters

The formula for the transfer function $T(s)$ is now known as *Mason's Gain Formula*. Equation A.1 is the formula to obtain this function, where $C(s)$ is the output and $R(s)$ the input of the transfer function. In this application $C(s)$ is the either Z or X, depending if we are interested in the main- or the add-on piston, $R(s)$ is the disturbance (δ). Δ_i is obtained from Δ by removing the loops which are touching the *i-th* forward path. P_i is the gain of the *i-th* forward path.

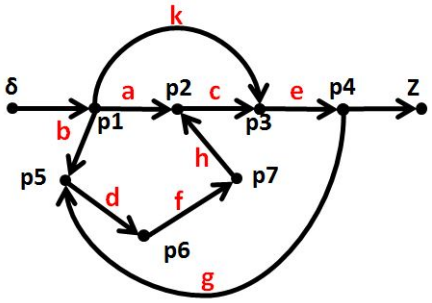

(a) Signal Flow Graph - Z

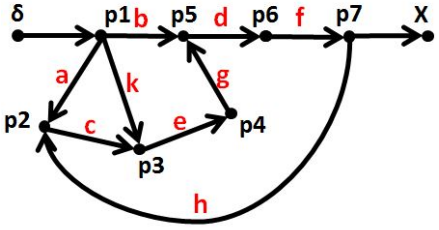

(b) Signal Flow Graph - X

Table A.1: Setup settings

a	A_g
b	A_g
c	$\frac{p_0}{V_0}A_p$
d	$\frac{p_0}{V_0}A_a$
e	G_z
f	G_x
g	$-A_p$
h	$-A_a$
k	G_d

$$T(s) = \frac{C(s)}{R(s)} = \frac{\sum_{i=1}^{N} P_i \Delta_i}{\Delta} \tag{A.1}$$

$$\Delta = 1 - \sum (IndividualLoopgains) + \sum (ProductsPossibleTwoNonTouchingloops) - \sum (ProductsPossibleThreeNonTouchingloops) + ... \tag{A.2}$$

$$Gx = \frac{1}{m_t s^2 + c x_t s + k x_t} \tag{A.3}$$

$$Gz = \frac{1}{M_t s^2 + c z_t s + k z_t} \tag{A.4}$$

$$Gd = \frac{\frac{Ag}{Ap} c z_t s + \frac{Ag}{Ap} k z_a}{1} \tag{A.5}$$

A.2.1 Derivation for Z

First all the forward paths are computed, it can be observed in figure A.2a that there are three (N = 3). The paths are:

1. $p1 \rightarrow p2 \rightarrow p3 \rightarrow p4$ **[a c e]**

2. $p1 \rightarrow p3 \rightarrow p4$ **[k e]**
3. $p1 \rightarrow p5 \rightarrow p6 \rightarrow p7 \rightarrow p2 \rightarrow p3 \rightarrow p4$ **[b d f h c e]**

There is one loop present in the system ($L = 1$):

1. $p2 \rightarrow p3 \rightarrow p4 \rightarrow p5 \rightarrow p6 \rightarrow p7 \rightarrow p2$ **[d f h c e g]**

Since there is only one loop the computation of Δ is straightforward. (Equation A.2) Since the loop touches all forward paths Δ_1,Δ_2,Δ_3 (N=3) are all 1.

$$\frac{Z}{\delta} = \frac{\sum_{i=1}^{N} P_i \Delta_i}{\Delta} = \frac{ace(1) + bdfhce(1) + ke(1)}{1 - gdfhce} = \frac{ace + bdfhce + ke}{1 - gdfhce}$$

$$= \frac{A_g \frac{p_0}{V_0} A_p G_z - A_g \frac{p_0}{V_0} A_a G_x A_a \frac{p_0}{V_0} A_p G_z + G_d G_z}{1 - A_p \frac{p_0}{V_0} A_a G_x A_a \frac{p_0}{V_0} A_p G_z} = \frac{A_g A_p \frac{p_0}{V_0} G_z - A_g A_p \left(A_a \frac{p_0}{V_0}\right)^2 G_x G_z + G_d G_z}{1 - \left(A_a A_p \frac{p_0}{V_0}\right)^2 G_x G_z} \tag{A.6}$$

A.2.2 Derivation for X

With the same steps as the derivation of the transfer-function $\frac{Z}{\delta}$ is done, $\frac{X}{\delta}$ is calculated. Only the results of each step are shown below.
N = 3

1. $p1 \rightarrow p5 \rightarrow p6 \rightarrow p7$ **[b d f]**
2. $p1 \rightarrow p2 \rightarrow p3 \rightarrow p4 \rightarrow p5 \rightarrow p6 \rightarrow p7$ **[a c e g d f]**
3. $p1 \rightarrow p3 \rightarrow p4 \rightarrow p5 \rightarrow p6 \rightarrow p7$ **[k e g d f]**

L = 1

1. $p5 \rightarrow p6 \rightarrow p7 \rightarrow p2 \rightarrow p3 \rightarrow p4 \rightarrow p5$ **[d f h c e g]**

$$\frac{X}{d_{in}} = \frac{bdf + acegdf + kegdf}{1 - hcegdf} = \frac{A_g \frac{p_0}{V_0} A_a G_x + A_g \frac{p_0}{V_0} A_p G_z (-A_p) \frac{p_0}{V_0} A_a G_x + G_d G_z (-A_p) \frac{p_0}{V_0} A_a G_x}{1 - (-A_a) \frac{p_0}{V_0} A_p G_z (-A_p) \frac{p_0}{V_0} A_a G_x}$$

$$= \frac{A_g A_a \frac{p_0}{V_0} G_x - A_g A_a \left(A_p \frac{p_0}{V_0}\right)^2 G_x G_z - A_p A_a \frac{p_0}{V_0} G_d G_x G_z}{1 - \left(A_a A_p \frac{p_0}{V_0}\right)^2 G_x G_z} \tag{A.7}$$

Appendix B

Negative Stiffness

B.1 Introduction

In this appendix the negative stiffness implementation at the main piston is discussed. This is required for the validation of the model of chapter 5 and is implemented in the design of the demonstrator (chapter 6). The concept is discussed B.2, the derivation of formulas is covered in section B.3. The effect this negative stiffness will have on the system is discussed in section B.4. A potential improvement is shown in section B.5.

B.2 Concept

To achieve the negative stiffness, a spring configuration is used. A visualisation is shown in B.1a, in this thesis the vertical spring is a representation for the airpot. Springs are compressed, thus storing energy, and will exert a force. If the spring compression is perfectly horizontal, only force in x-direction will be exerted. However if there is a slight angle a force component will be exerted in z-direction, which will try to move the point out of its initial position. If we use 3 springs, as shown in figure B.1b, the system will is balanced in plane. (No instability in the out of plane direction y). The three springs create an unstable equilibrium at the working point with a negative stiffness range in the z-direction.

B.3 Modelling of the negative stiffness

For this setup simple formulas are used; with L_0 the initial spring length; L_p the pre-tensioning distance and k_{spring} the spring constant of the 3 (identical) springs. The parameters are visualized in figure B.2.

$$F_{spring} = \left(L_0 - \sqrt{\left(L_0 - L_p\right)^2 + \mathrm{d}z^2} \right) \cdot k_{spring} \tag{B.1}$$

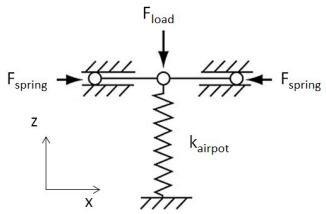

(a) A mechanical solution to vibration isolation, as discussed in 3.2.2. (Figure derived from [15])

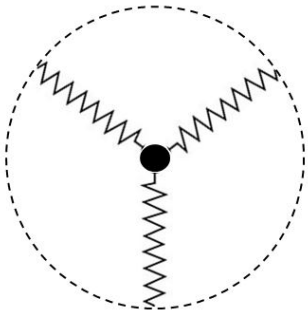

(b) Stability due to spring configuration

Figure B.1: Visualisation of the negative stiffness concept

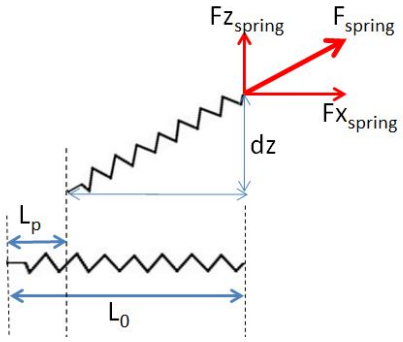

Figure B.2: Visualization of the different parameters used in the formulas for the negative stiffness concept.

$$Fz_{spring} = \sin\left(\arctan\left(\frac{\mathrm{d}z}{L_0 - L_p}\right)\right) \cdot F \tag{B.2}$$

B.4 Effect on the airpot

Using the characteristics of the airpot and the calculations shown in B.3 figures B.4a and B.4bare obtained. It can be observed that the stiffness is lowered considerably (from *kp* to *Summation*) at the operating point (vertical displacement is zero). This will result in a decrease in eigen-frequency. However even in theory this is only exactly at the intended operating point, if the system does not act exactly at its operating point, the effect is already reduced significantly. An additional option to increase this range is shown in section B.5.

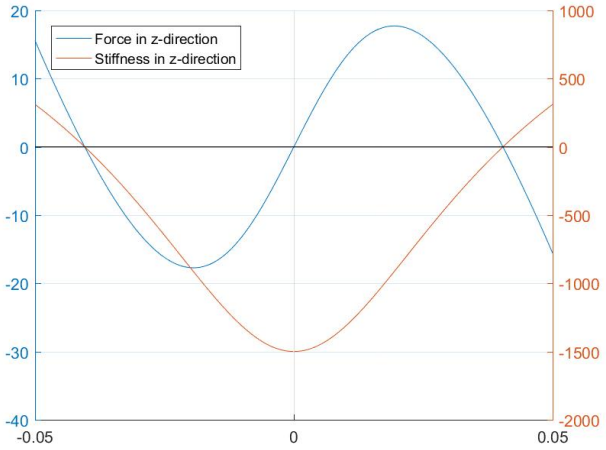

Figure B.3: MATLAB-model result for the described 3-spring configuration.
($M = 10\,\text{kg}, D_p = 0.08\,\text{m}, D_g = 0.09\,\text{m}, L_0 = 0.0508\,\text{m}, L_p = 0.02\,\text{m}, k_s = 770\,\text{N/m}$)

B.5 Potential Improvement

To improve the range of constant negative stiffness a small change to the setup could be used. By offsetting the fixed world side off the springs in the "z" direction and using a different pre-tension for the springs one can tune the negative stiffness range. An example is given in figure B.6, which is created using the values in table B.1. However since the springs are no longer used symmetrically, a moment is introduced upon the system. This moment should be taken into account as it will affect the alignment of the piston.

	L_p [mm]	z_{off} [mm]
S1	10	0
S2	30	-15
S3	30	15

Table B.1: Parameters for the alternative spring configuration. z_{off} is the distance of the springs connection to the frame from the operating point. $k_s = 770\,\text{N/m}, L_0 = 0.508\,\text{m}$

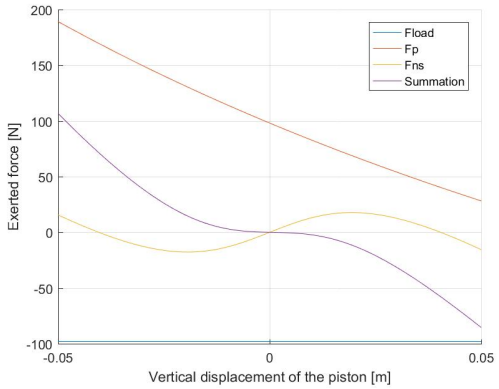

(a) Visualisation of all acting forces and their summation

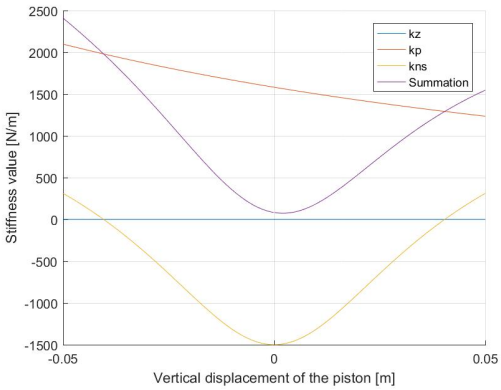

(b) The individual stiffness's and their summation

Figure B.4: Effect on airpot performance.
($M = 10\,\mathrm{kg}, D_p = 0.08\,\mathrm{m}, D_g = 0.09\,\mathrm{m}, L_0 = 0.0508\,\mathrm{m}, L_p = 0.02\,\mathrm{m}, k_s = 770\,\mathrm{N/m}$).

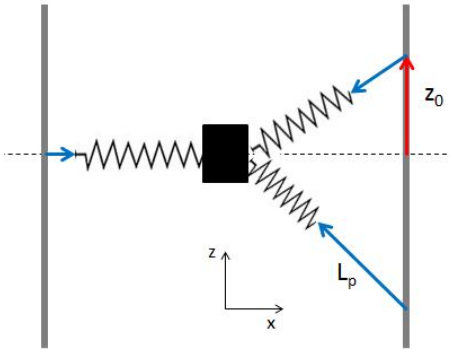

Figure B.5: A visualisation of parameters of the alternative spring configuration. This is a 2-dimensional representation of the side-view of the system. (The springs are placed 120° around the z-axis as described B.1b).

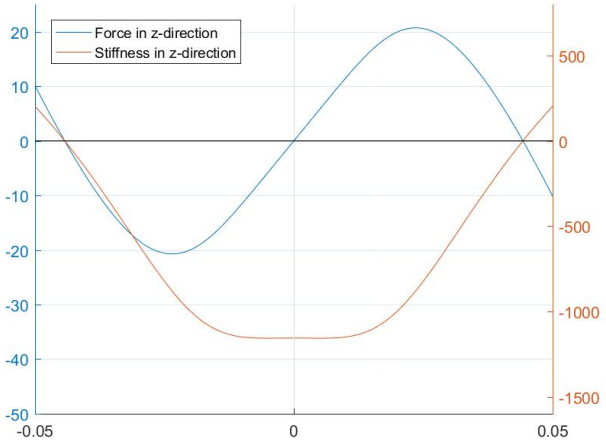

Figure B.6: MATLAB-model result for the alternative 3-spring configuration. (section B.5. Values for the alternative spring placement are shown table B.1
($M = 10\,\mathrm{kg}, D_p = 0.08\,\mathrm{m}, D_g = 0.09\,\mathrm{m}, L_0 = 0.0508\,\mathrm{m}, k_s = 770\,\mathrm{N/m}$)

Appendix C

Model verification

C.1 Validation

The model was gut-feeling tested in advance by changing 1 of the parameters en see what happens in the model and if it corresponds to the expectations. As a starting point the model was compared with the standard air-spring characteristic. Thus the add-on is not yet present in the first part. (Situation of figure C.1a.

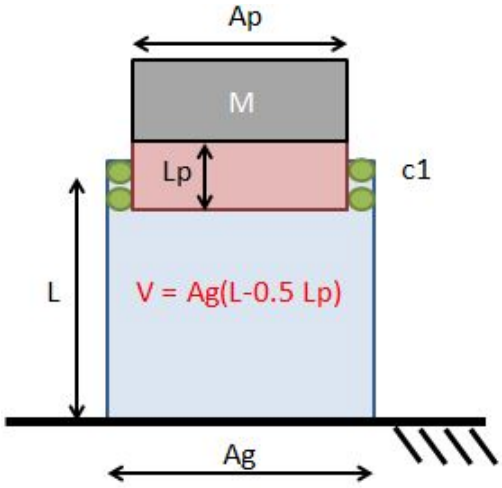

(a) Signal Flow Chart

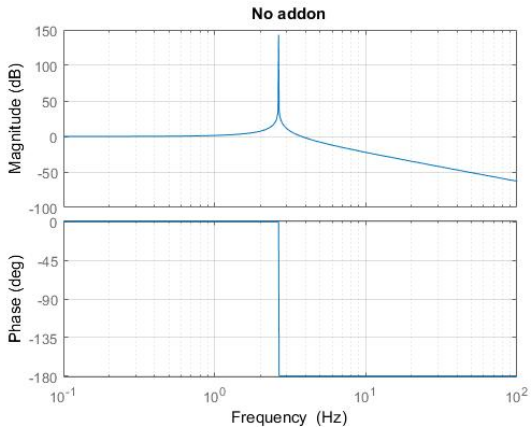

(b) Standard air spring response with the given parameters of table C.1

Figure C.1: Flow chart model check

These parameters are fixed for a current solutions, thus these can be chosen to resemble an existing product, but have no variations further in this research since they are not part of the add-on. Thus $L, L_p, c1, Ap\&M$ are fixed and will resemble the reference value for the testing phase.

With the parameter values given in table C.1 figure C.1b is obtained from the model. In which

Table C.1: Initial parameter values

	Dimension	Description
M	20 kg	Total mass of load & piston
L	0.2 m	Pot Length
L	5 cm	Piston Length
A_p	9 cm^2	Area of load carrying piston
A_a	3 cm^2	Area of the add-on

we see a resonance peak at 2.6 Hz and a -2 slope after the peak.

From the section on the flow graph theory we obtained a model for the system with add-on. To check if this model is valid the parameters of the add-on are added one by one to see if the expected changes in the response occur. If they do not, we have to see what might be the problem: the model or the expected result.

Chart Flow Model check for single piston system First both models are compared for the one piston result. Since both models, the basic model and the model obtained by the flow chart theory are capable of describing the response of the single piston system. The result without and with damping are shown in figure C.2a and C.2b. As can be seen in the plots, the result is the same, which indicates the model is valid.

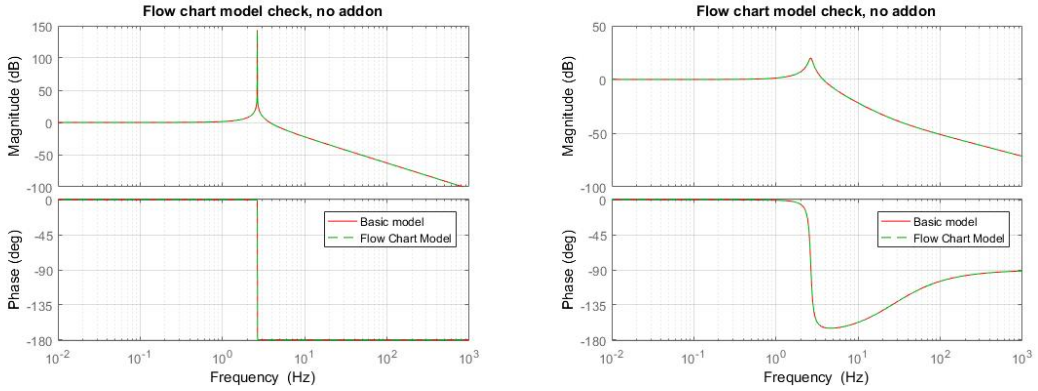

(a) Without damping (b) With damping

Figure C.2: Model comparison

Two half masses on half surface The first test was if the system would yield the same result if we would have 2 $\frac{M}{2}$ masses on areas of $\frac{A}{2}$, as shown in figure C.3a. This is indeed the case, as can be seen in figure C.3b. There is a change, namely that an extra resonance-peak occurs, this is the situation that only one piston would be moving and the other stands still; in this situation only one piston cancels the vibration. Thus the model does as was expected.

Model variations As the system is designed as an add-on, parameters of the airpot itself are taken as constant during these parameter variations, only the parameters of the add-on will be varied. Dimensions of the airpot are chosen such that a fabrication of a test setup is easy.

As a first step for the 2 piston concept the second piston is chosen identical to the load-carrying piston. This results in figure C.4a. From this figure two observations can be made if we compare

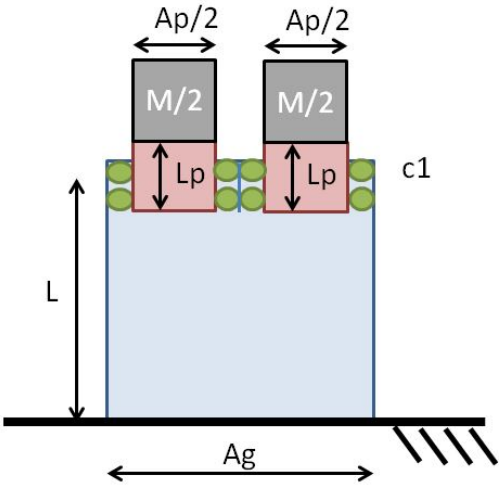

(a) Small test 2 pistons

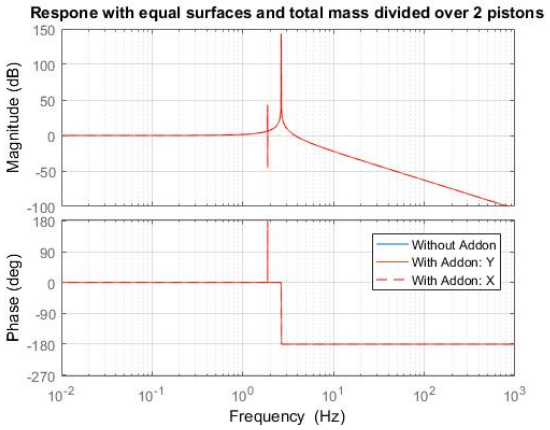

(b) Signal Flow Chart

Figure C.3: 2 pistons, halved mass, halved surface

it with figure C.2a: first the magnitude of the response at low frequencies is lowered, secondly the eigenfrequency of the system is shifted to the right.

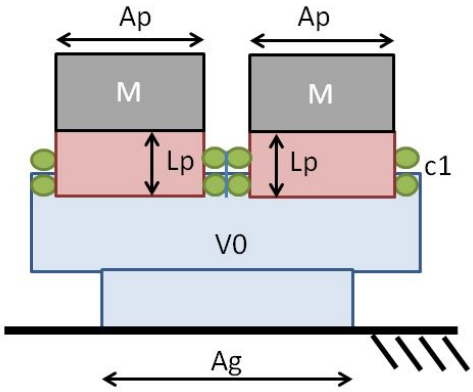

(a) Small test 2 pistons

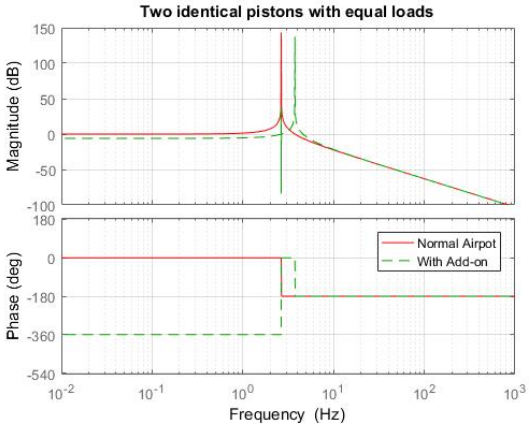

(b) Signal Flow Chart

Figure C.4: 2 pistons, both with the same area and the same mass

The magnitude of the response at low frequencies is halved (-6 dB) because we have two identical pistons instead of one, both pistons are only forced to due halve the work. The increase of the eigenfrequency is explained that if both pistons would act equally, the system has essentially a twice as large mass on a twice as large surface. With $k = \frac{pA^2}{V0} = \frac{[1][2]^2}{[1]} = 4$ and $f_n = \sqrt{\frac{k}{m}} = \sqrt{\frac{[4]}{[2]}}$ the eigenfrequency is shifted a factor $\sqrt{2}$ to the right.

The addon has a couple of parameters that can be changed, these are listed below, the effect of

changing the parameters is discussed in this section.

- Aa - The area of the add-on piston
- m - The mass of the moving piston
- k_ext - An external spring to adjust the add-on
- cx - The damping of the add-on

Changing the mass; we can observe that for the lower masses of the add-on, the low frequency response is improved considerably (in the no-damping situation). But also that the response peak of the combined movement is shifted to the right (lower mass in $\sqrt{k/m}$), this could lead to problems in the higher frequency domains (which is a problem not present in the current systems on the market).

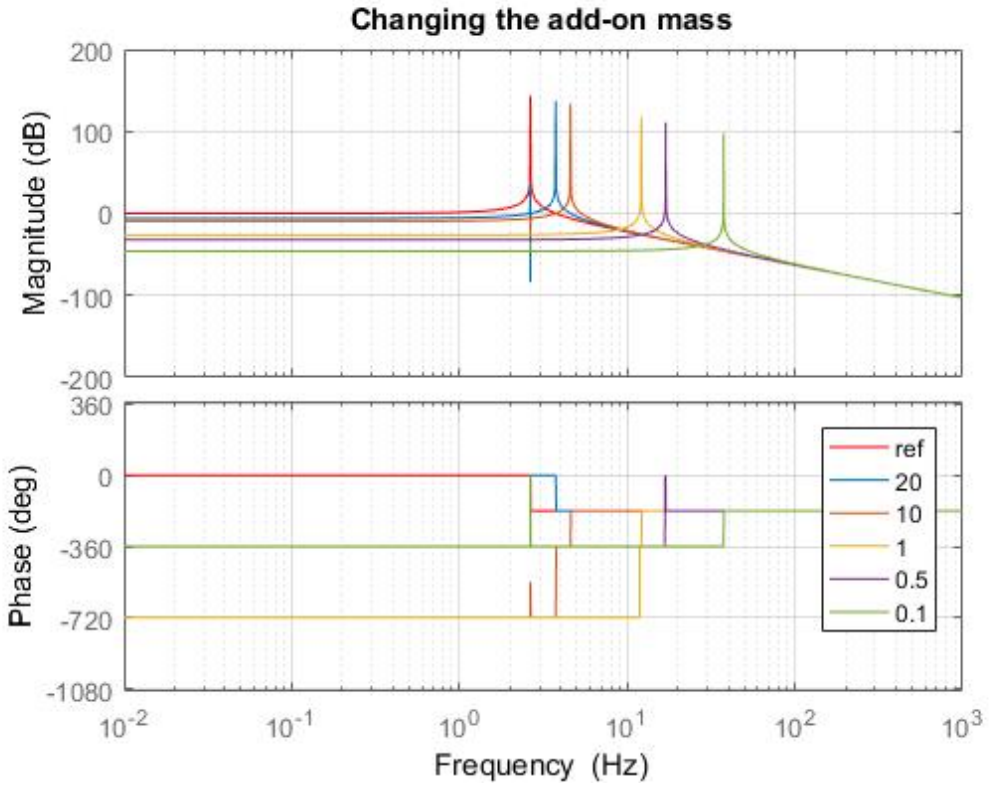

Figure C.5: Changing the add-on mass.

Changing the add-on area; it can be observed that the effect of the add-on is larger with larger add-on area. However in the legend the required force at the add-on is also displayed, which gets considerably larger with increase in the add-on area.

Changing the damping of the add-on; the effect at lower frequencies is gone if we have damping at the add-on (and not at the load carrying piston). Also we observe that the load-carrying piston

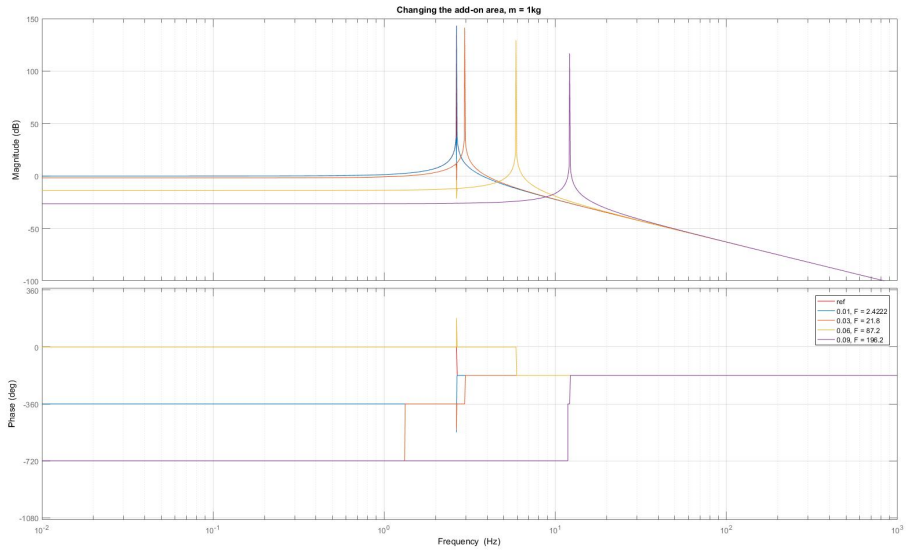

Figure C.6: Changing the add-on area.

can be damped at it's eigenfrequency by just damping the add-on. While still maintaining a -2 slope at the higher frequencies. (Damping of the load-carrying piston will result in a -1 slope).

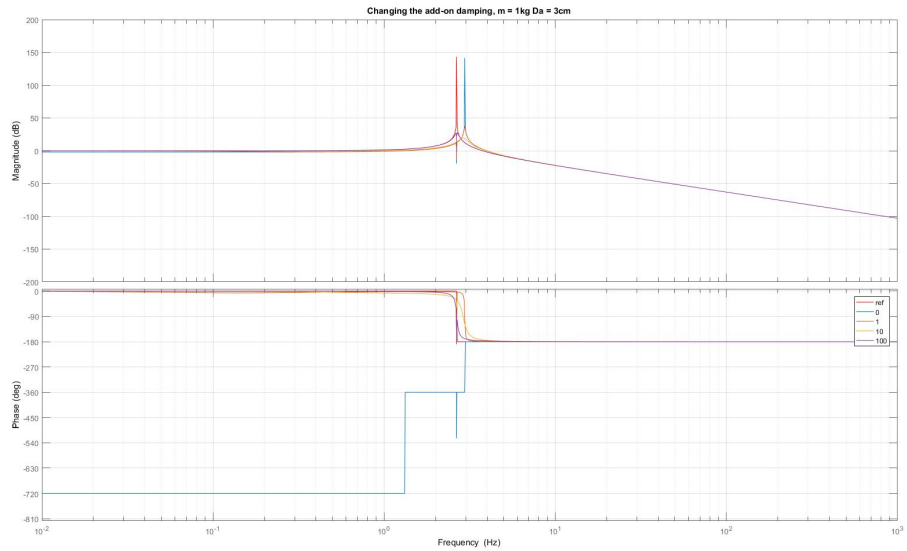

Figure C.7: Changing the add-on Damping.

External spring Until now the only spring constant present at the add-on was that of the add-on moving against the air inside the pot. But this will most likely not be the only spring factor, because of two items:

- Instability. A very small force-change at the load would push the add-on towards the ends of this range (and towards eventual stoppers). This will cause undesirable effects. Therefore a small k value would be able to hold the system around its desired position even if small deviations of force are present.
- Multi-stability. If constant force at the add-on is achieved, and also there are no deviations in the force coming from the load, the system will have multiple stable positions (every point of the constant force-range). The problem with this is that the system may choose a set-point to close to the stoppers, which might also cause problems again.

Adding damping to the load carrying piston From literature, a normal value for the damping coefficient is ≈ 0.05. If we apply this to our system a damping value of $\approx 33\,\mathrm{Ns/m}$ is obtained.

Appendix D

Additional Graphs

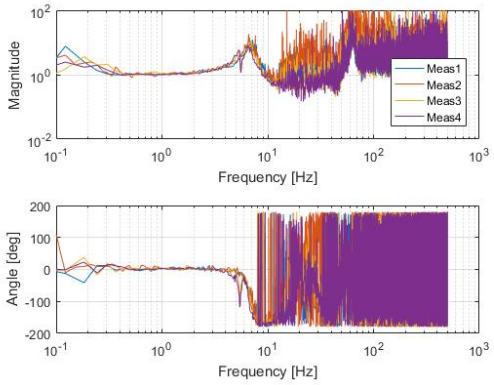

(a) Measurement results with a load mass of 2 kg

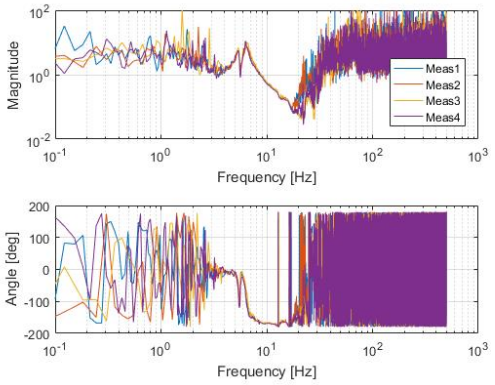

(b) Measurement results with a load mass of 2 kg

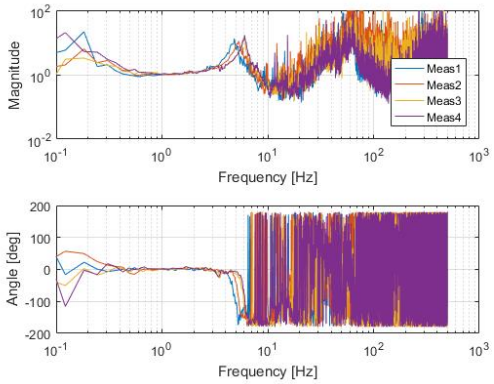

(c) Measurement results with a load mass of 6 kg

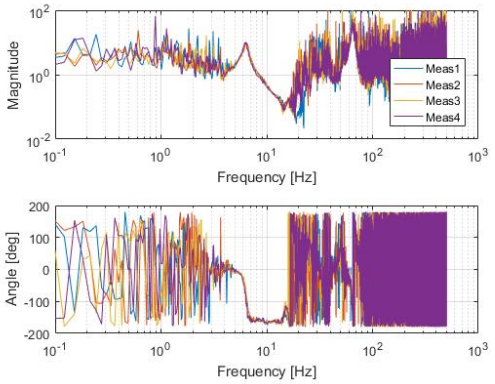

(d) Measurement results with a load mass of 6 kg

Figure D.1: Measurement results for different loads and actuation. a) and c) are self actuated. b) and d) are actuated with the shaker.

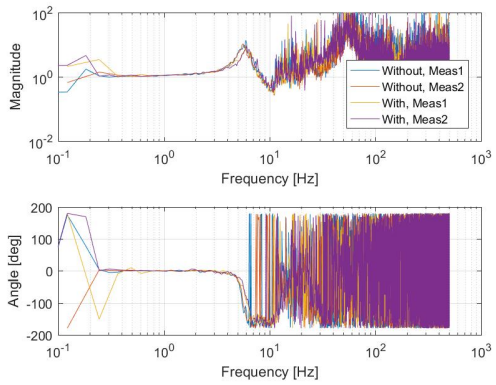

(a) Measurement results with a load mass of 2 kg, self actuated (low frequency)

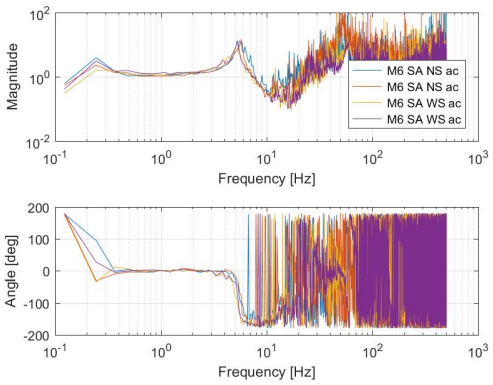

(b) Measurement results with a load mass of 6 kg, self actuated (low frequency)

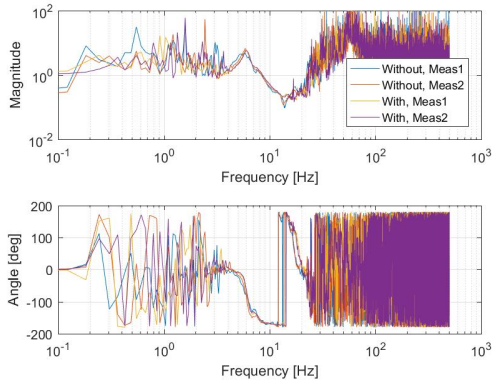

(c) Measurement results with a load mass of 2 kg, actuated with the shaker

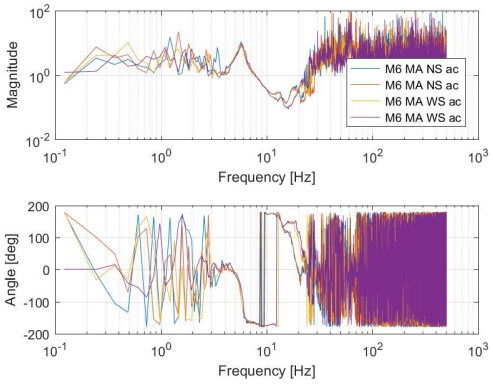

(d) Measurement results with a load mass of 6 kg, actuated with the shaker

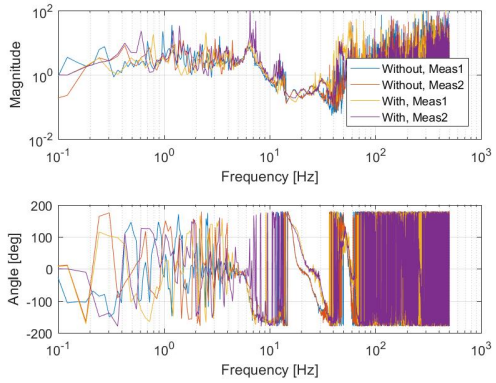

(e) Measurement results with a load mass of 2 kg, actuated with the shaker (high frequency)

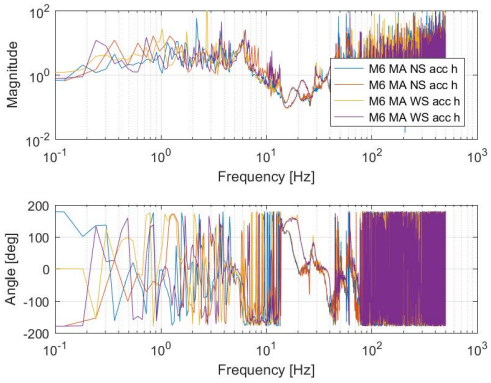

(f) Measurement results with a load mass of 6 kg, actuated with the shaker (high frequency)

Figure D.2: Measurement results for negative stiffness comparison

Appendix E

Design in SolidWorks

E.1 Introduction

In this appendix the different sub-assemblies are shown as well as that of the full system.

E.2 Spring configuration

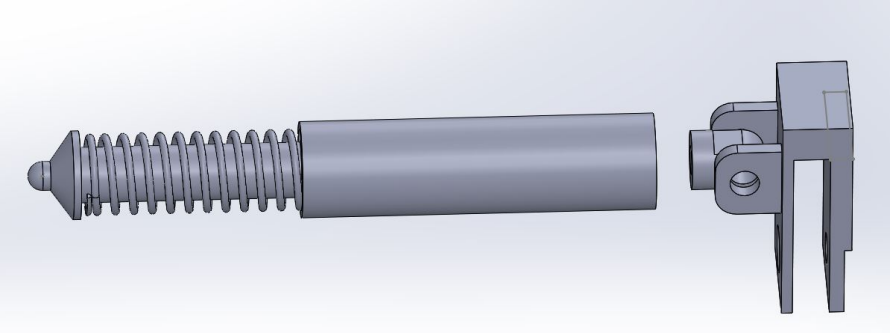

Figure E.1: Design of the spring configuration in SolidWorks.

Figure E.2: Design of the main piston configuration in SolidWorks.

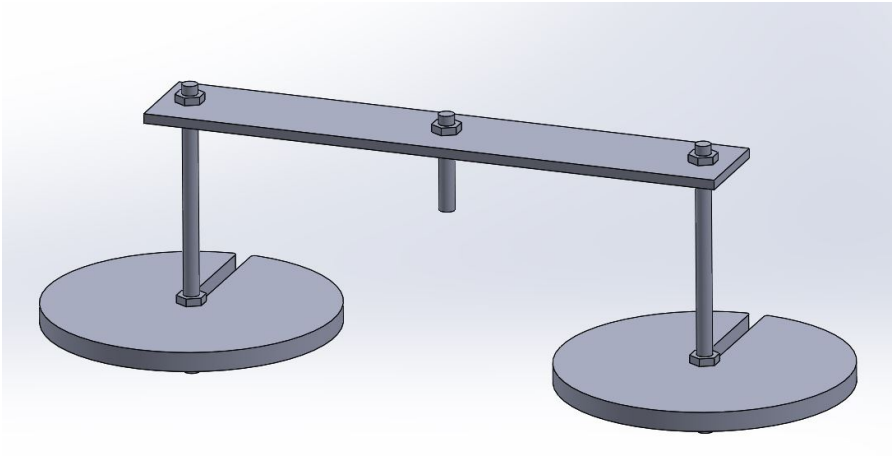

Figure E.3: Design of the load subsystem in SolidWorks.

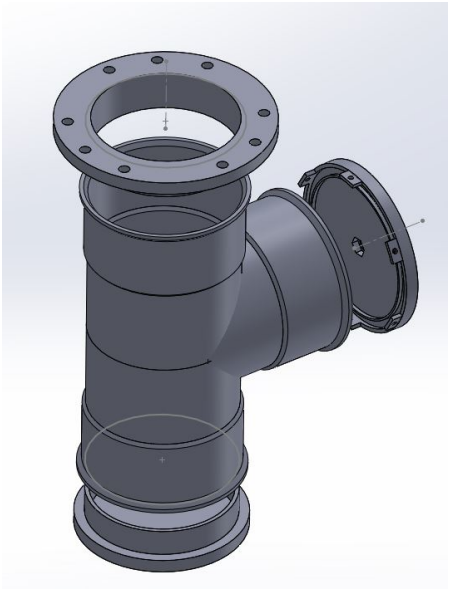

Figure E.4: Design of the frame configuration in SolidWorks.

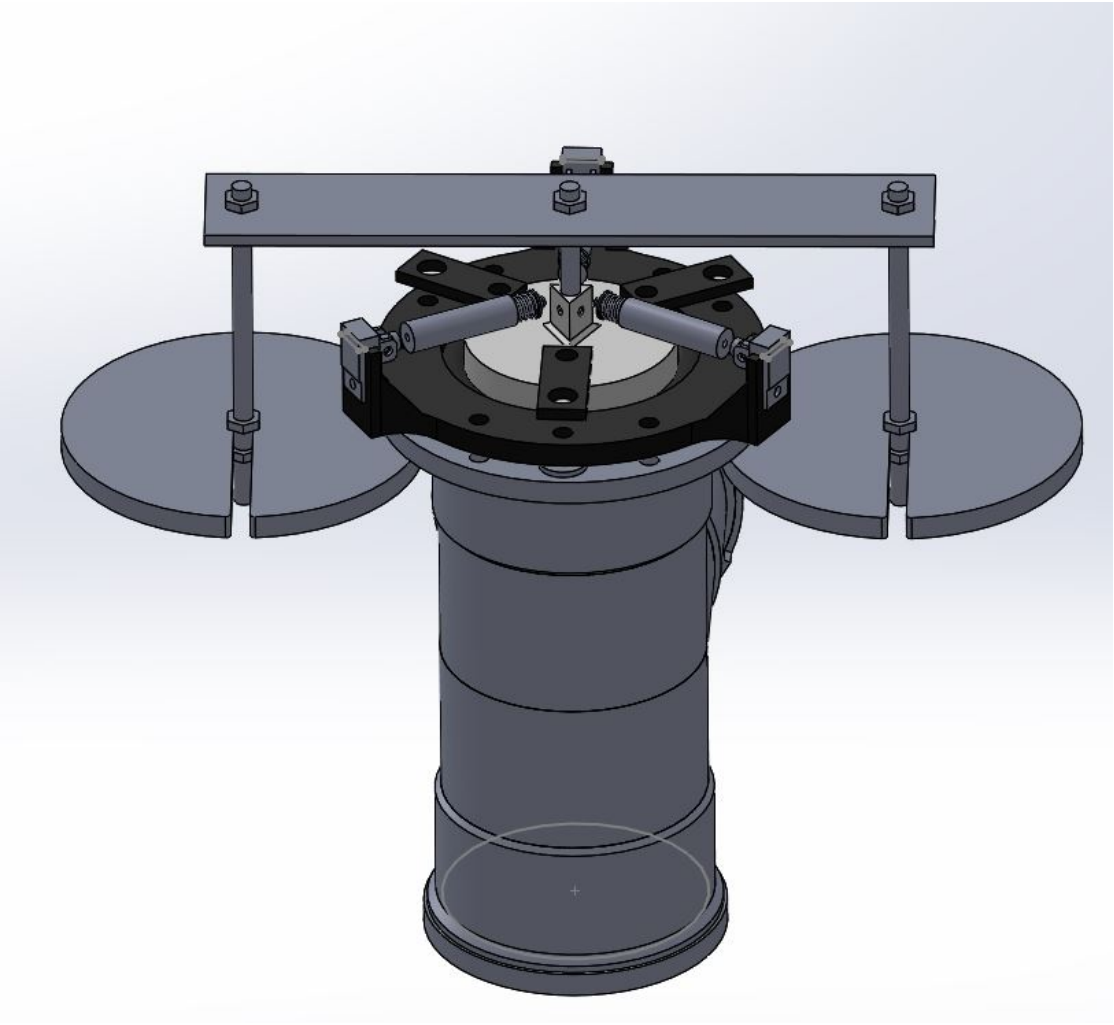

Figure E.5: Design of the frame configuration in SolidWorks.

Appendix F

Preliminary ideas for add-on design

F.1 Introduction

In the starting phase of this research work modelling of the full system and design of the add-on was done simultaneously. After some time the decision was made to focus on the model first as its results would have effect on a potential design of the add-on. However to let the work done not fully disappear some of the designs considered in this research phase are shown in this appendix. These are not fully calculated designs but are simply to give potential new research into this subject some ideas as a starting point.

F.2 Concepts for the add-on

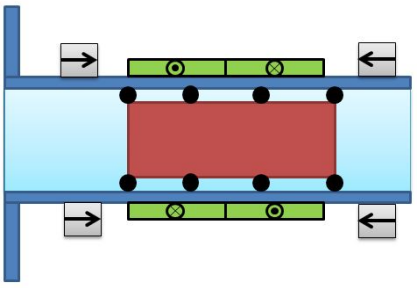

Figure F.1: A concept for a magnetic add-on

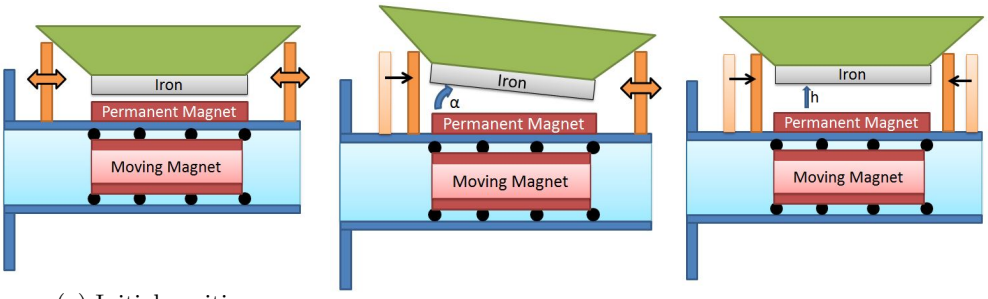

(a) Initial position (b) Tunable angle (c) Tunable height

Figure F.2: A concept for a tunable magnetic add-on

F.3 Design concepts full system

Design 1 The magnetic solution is shown with a linear guide. As an potential solution a ferro-fluid bearing is used to seal the inner pressure while having low friction. Potential issues arise with large overpressure between inside and the ambient pressure and the capability of the sealing using ferro-fluid.

Design 2 To overcome the pressure-difference issue, an additional volume is introduced. This volume should have almost the same pressure as the airspring as to prevent large pressure differences at the seal. However using this additional volume requires 2 systems to be pressurized. Also the added volume will work as an additional spring on the right-hand side (of figureF.3b) of the moving mass.

Design 3 To prevent the pressurization of 2 volumes, a bypass can be used to allow both volumes to be pressurized at the same time. This bypass should have large damping for high frequencies as to not disturb the vibration isolation capabilities of the system.

Design 4 The drawn bypass of stage 3 is now implemented inside the valve this is a more elegant solution than the bypass shown in figure F.3c.

Design 5 This design shows the option of placing the add-on inside the airspring, while also having the additional volume in a compact matter. However due to the orientation of the add-on gravity will also work on the bottom piston, potentially only worsening the airpot performance.

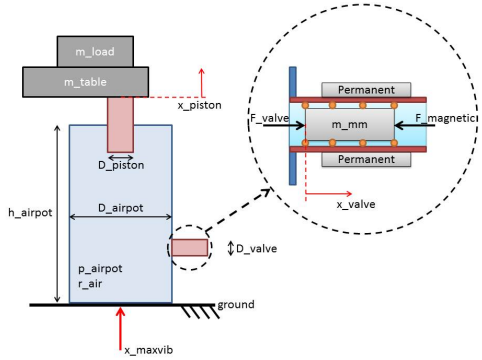

(a) Design 1

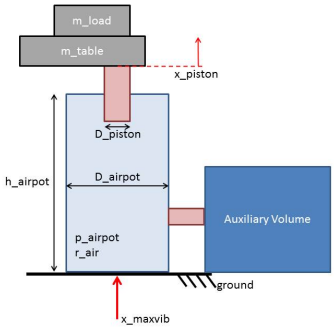

(b) Design 2

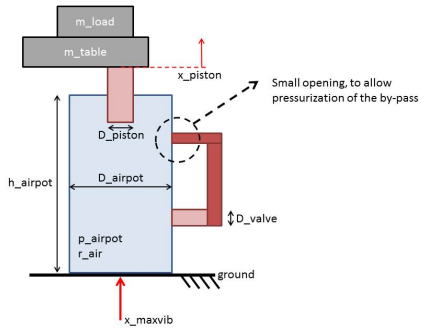

(c) Design 3

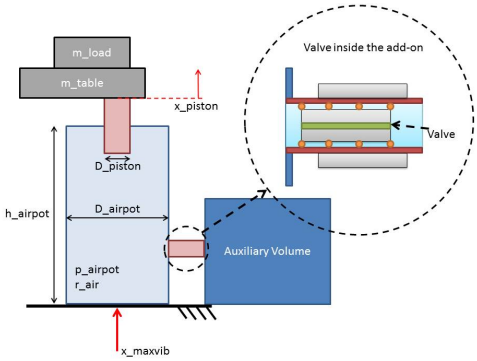

(d) Design 4

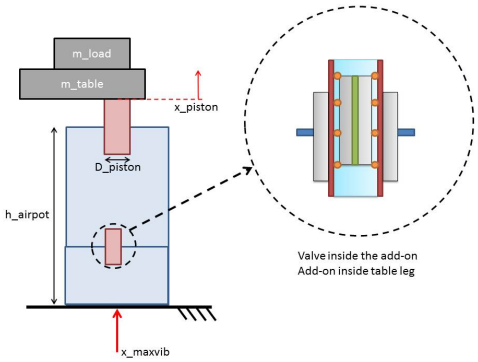

(e) Design 5

Figure F.3: Stages of the design

Appendix G

Matlab Codes

G.1 Introduction

In this appendix Matlab codes are shown of the most important m-codes used for this thesis.

G.2 Transmissibility Function

To calculate the transmissibility functions based on different parameters a function file was created.

```
function [sys_x,sys_y] = NV_detTF_side(m,Aa,kx_p,cx_p,kx_a,cx_a)
global Ag Ap M kz_p kz_a cz_p cz_a p0 V0
kz_t = kz_p+kz_a;
cz_t = cz_p+cz_a;
kx_t = kx_p+kx_a;
cx_t = cx_p+cx_a;

Gz = tf(1, [M cz_t kz_t]);

if m == 0
Gx = 0;
else
Gx = tf(1, [m cx_t kx_t]);
end

Gd = tf([Ag/Ap*cz_p Ag/Ap*kz_a],1);

% Flow chart model parameters
a = Ag;
b = Ag;
c = p0/V0*Ap;
d = p0/V0*Aa;
e = Gz;
f = Gx;
g = -Ap;
h = -Aa;
```

```
k = Gd;

sys_y = (a*c*e + b*c*d*e*f*h + k*e)/(1-c*d*e*f*g*h);
sys_x = (b*d*f + a*c*e*g*d*f + k*e*g*d*f)/(1-c*d*e*f*g*h);
```

G.3 Negative Stiffness Calculation

```
L1 = preT;
L2 = preT;
L3 = preT;

rangPlt = 0.05; % Plot range +/- m
step = 0.0001;
off = 0;

dz = -rangPlt:step:rangPlt;
dz2 = dz+off;
dz3 = dz-off;

F1 = (L0-sqrt((L0-L1)^2+dz.^2))*k;
F2 = (L0-sqrt((L0-L2)^2+dz2.^2))*k;
F3 = (L0-sqrt((L0-L3)^2+dz3.^2))*k;
Ftot = F1 + F2 + F3;

F1z = sind(atand(dz./(L0-L1))).*F1;
F2z = sind(atand(dz2./(L0-L2))).*F2;
F3z = sind(atand(dz3./(L0-L3))).*F3;
Ftotz = F1z+F2z+F3z;

k1z = -F1z./dz;
k2z = -F2z./dz2;
k3z = -F3z./dz3;
Ktot = -(F1z+F2z+F3z)./dz;
%% Airpot
global Ag Ap M cy ky p0 V0

% Initial calculations
Ag = (Dg/2)^2*pi;           % Area airpot
Ap = (Dp/2)^2*pi;           % Area piston
rat = Ag/Ap;                % Area ratio airpot/piston
Vg = Ag*L;                  % Volume airpot
% Vg_adj = Vg-0.5*Lp*Ap;    % Volume airpot, adjusted for piston
p_over = M*g/Ap;            % Required overpressure for equilibrium
p_in = p_over+p_amb;        % Total pressure inside

%
V0 = Vg;                % Chosen volume !! ADJUST !!
p0 = p_in;              % Calculated pressure
ky = p0*Ap^2/V0;        % Airspring stiffness at working point
ky_wc = r*p0*Ap^2/V0;   % Airspring stiffness including compressibility

% Combined forces
p_new = p0*V0./(V0+dz.*Ap);
Fp = Ap*(p_new-p_amb);
Fload = -ones(1,length(Fp))*M*g;
Fns = Ftotz;
```

```
%% Improvement on negative stiffness range
% Pretensioning distance
preT = 0.03;   % [m]
L1 = preT-0.2*preT;
L2 = preT;
L3 = preT;

rangPlt = 0.05; % Plot range +/- m
step = 0.0001;
off = 0.015;

dz = -rangPlt:step:rangPlt;
dz2 = dz+off;
dz3 = dz-off;

F1 = (L0-sqrt((L0-L1)^2+dz.^2))*k;
F2 = (L0-sqrt((L0-L2)^2+dz2.^2))*k;
F3 = (L0-sqrt((L0-L3)^2+dz3.^2))*k;
Ftot = F1 + F2 + F3;

F1z = sind(atand(dz./(L0-L1))).*F1;
F2z = sind(atand(dz2./(L0-L2))).*F2;
F3z = sind(atand(dz3./(L0-L3))).*F3;
Ftotz = F1z+F2z+F3z;

% To show that the forces in x-direction are no longer equal
F1x = cosd(atand(dz./(L0-L1))).*F1;
F2x = cosd(atand(dz2./(L0-L2))).*F2;
F3x = cosd(atand(dz3./(L0-L3))).*F3;
Ftotx = F1x+F2x+F3x;

k1z = -F1z./dz;
k2z = -F2z./dz2;
k3z = -F3z./dz3;
Ktot = -(F1z+F2z+F3z)./dz;
```

G.4 Data processing

```
%% Insert Data file
[filename, pathname, filterindex] = uigetfile('*.txt', 'Pick a TEXT code file');
file = [pathname,filename];

T = importdata(file);

%% Data load
t = T(:,1)';    % Time vector
c1 = T(:,2)';   % Accelerometer 1: +
c2 = T(:,3)';   % Accelerometer 1: -
c3 = T(:,4)';   % Accelerometer 2: +
c4 = T(:,5)';   % Accelerometer 2: -
c5 = T(:,6)';   % Pressure sensor
Ts = t(2)-t(1);
Fs = 1/Ts;

%% Translation to real values
A1p = c1-mode(c1);
A1m = c2-mode(c2);
A2p = c3-mode(c3);
A2m = c4-mode(c4);
```

```
p = (((c5./0.466)-4).*2.5./16)+1;   % [bar]

%% Combined signal +/-
A1 = A1p-A1m;
A2 = A2p-A2m;

%% Calculate transferfunction
[pxy, fp] = cpsd(A2,A1,[],[],[],Fs);
[pyy, fp2] = pwelch(A1,[],[],[],Fs);
H2 = pyy./pxy;
H2_mag = abs(H2);
H2_pha = rad2deg(angle(H2));
```

G.5 calcH2: Automatized data handling file:

```
%% Nils Velders
% Automized data handling. Returns H2 for different inputs.

function [H2_mag, H2_pha, fp, H2_pha_w, H2_pha_adj, filename] = calcH2(fmin,fmax,filtervalue,phase

if ~exist('fmin','var') || isempty(fmin),
fmin = 1;
end
if ~exist('fmax','var') || isempty(fmax),
fmax = 25;
end
if ~exist('filtervalue','var') || isempty(filtervalue),
filtervalue = 1;
end
if ~exist('phasefil','var') || isempty(phasefil),
phasefil = 100;
end

%% FileSelection
[filename, pathname, ~] = uigetfile('*.txt', 'Pick a TEXT code file');
file = [pathname,filename];

T = importdata(file);

%% Data load
t = T(:,1)';    % Time vector
c1 = T(:,2)';   % Accelerometer 1: +
c2 = T(:,3)';   % Accelerometer 1: -
c3 = T(:,4)';   % Accelerometer 2: +
c4 = T(:,5)';   % Accelerometer 2: -
Ts = t(2)-t(1);
Fs = 1/Ts;

%% Translation to real values
A1p = c1-mode(c1);
A1m = c2-mode(c2);
A2p = c3-mode(c3);
A2m = c4-mode(c4);

%% Combined signal +/-
A1 = A1p-A1m;
A2 = A2p-A2m;

%% Calculate H2
```

```
[pxy, fp] = cpsd(A2,A1,[],[],[],Fs); % cpsd(A2,A1);
[pyy, ~] = pwelch(A1,[],[],[],Fs); % pwelch(A1);

H2 = pyy./pxy;

H2_mag = abs(H2);
H2_pha = rad2deg(angle(H2));
start_wrap = find(fp>fmin,1);
end_wrap = find(fp>fmax,1);

H2_pha_wrapped = rad2deg(unwrap(angle(H2(start_wrap:end_wrap)),filtervalue*pi));
H2_pha_w = H2_pha;
H2_pha_w(start_wrap:end_wrap) = H2_pha_wrapped;

H2_pha_adj = zeros(size(fp));
for i = 1:length(fp)
if H2_pha(i)>phasefil
H2_pha_adj(i) = NaN;
else
H2_pha_adj(i) = H2_pha(i);
end
end
```

G.6 compareN(n): automized file to compare N-data sets

```
function [] = compareN(n)
%%

for i = 1:n
[H2_mag, H2_pha, fp, H2_pha_w, H2_pha_adj, file] = calcH2();

DataNo = strcat('D',num2str(i));
mag.(DataNo) = H2_mag;
pha.(DataNo) = H2_pha;
f.(DataNo) = fp;
phaW.(DataNo) = H2_pha_w;
phaA.(DataNo) = H2_pha_adj;
legendInfo{i} = file(18:end-4);
end

%%
figure
subplot(2,1,1)
for i = 1:n
DataNo = strcat('D',num2str(i)); %'H2_mag_',
f_temp = f.(DataNo);
mag_temp = mag.(DataNo);
loglog(f_temp, mag_temp)
hold on
end
grid on
xlabel('Frequency [Hz]')
ylabel('Magnitude')
legend(legendInfo)

subplot(2,1,2)
for i = 1:n
DataNo = strcat('D',num2str(i));
```

```
semilogx(f.(DataNo), pha.(DataNo))
hold on
end
grid on
xlabel('Frequency [Hz]')
ylabel('Angle [deg]')
```